Ply scale modelling of the quasi-static and fatigue behaviours of an acrylic-thermoplastic-matrix and glass-fibre-reinforced laminated composite covering the service temperature range of wind turbine blades

Eileen Boissin, Christophe Bois, Jean-Christophe Wahl, Thierry Palin-Luc, Damien Caous

Ply scale modelling of the quasi-static and fatigue behaviours of an acrylic-thermoplastic-matrix and glass-fibre-reinforced laminated composite covering the service temperature range of wind turbine blades

Eileen Boissin[1*], Christophe Bois[1], Jean-Christophe Wahl[1], Thierry Palin-Luc[2], Damien Caous[3]

1 : Université de Bordeaux, CNRS, Arts et Metiers Institute of Technology, Bordeaux INP, INRAE, I2M Bordeaux, F-33400 Talence, France

2 : Arts et Metiers Institute of Technology, CNRS, Université de Bordeaux, Bordeaux INP, INRAE, I2M Bordeaux, F-33405 Talence Cedex, France

3 : TENSYL

F- 17180 Perigny, France

eileen.boissin@u-bordeaux.fr, phone 33 5 56 84 79 85, fax: 33 5 56 84 58 43

christophe.bois@u-bordeaux.fr

jean-christophe.wahl@u-bordeaux.fr

thierry.palin-luc@ensam.eu

damien.caous@tensyl.com

Abstract

In this study, a model formulated at the ply scale was considered to describe the mechanical behaviour of an acrylic-thermoplastic-matrix and glass-fibre-reinforced laminated composite under monotonic tensile and fatigue loadings within a temperature range of -20°C to +60°C. This study showed that the temperature dependency of the composite transverse and off-axis mechanical behaviour could be determined concisely, by considering only the temperature dependency of the matrix initial elastic properties and keeping the parameters of the damage evolution laws constant. This is a relevant result for designing composite structures with a limited set of experimental data.

Keywords: Composite, Damage mechanics, Environmental effect, Fatigue modelling, Thermomechanical fatigue/cycling

$a\ (MPa^{-m})$	Damage model parameter driving matrix damage evolution under quasi-static loading according to transverse loading
$a_1\ (MPa^{-l_1-l_2})$	Damage model parameter driving fatigue damage in the fibre direction
$a_2\ (MPa^{-m_1-m_2})$	Damage model parameter driving matrix damage evolution under fatigue loading according to transverse loading
$b\ (MPa^{-n})$	Damage model parameter driving matrix damage evolution under quasi-static loading according to shear loading
$b_2\ (MPa^{-n_1-n_2})$	Damage model parameter driving matrix damage evolution under fatigue loading according to shear loading
$c\ (-)$	Proportionality coefficient between shear stiffness loss and stiffness loss in transverse direction
$d_1\ (-)$	Damage variable describing stiffness loss in fibre direction in the ply
$d_{12}\ (-)$	Damage variable describing shear stiffness loss in the ply
$d_2\ (-)$	Damage variable describing transverse stiffness loss in the ply
$d_m\ (-)$	Damage model parameter within the coupling law between transverse stiffness loss d_2 and the ultimate thermodynamic force in the fibre direction Y_{d1}^{ult}
$d_\lambda\ (-)$	Damage model parameter within the coupling law between transverse stiffness loss d_2 and the ultimate thermodynamic force in the fibre direction Y_{d1}^{ult}
$E_D\ (MPa)$	Elastic strain energy at the ply scale
$E_f\ (MPa)$	Longitudinal Young modulus of fibres
$E_{ft}\ (MPa)$	Transverse Young modulus of fibres
$E_m\ (MPa)$	Young modulus of matrix
$E_1\ (MPa)$	Young modulus in fibre direction at the ply scale
$E_2\ (MPa)$	Young modulus in transverse direction at the ply scale
$f\ (-)$	Hardening function of the damage model driving plastic strain evolution
$G_f\ (MPa)$	Shear modulus of fibres
$G_m\ (MPa)$	Shear modulus of matrix
$G_{12}\ (MPa)$	Shear modulus at the ply scale
$K\ (MPa)$	Linear coefficient of the kinematic hardening law

$l_1\ (-)$	Power coefficient of the fatigue damage law associated with maximum thermodynamic force in the fibre direction
$l_2\ (-)$	Power coefficient of the fatigue damage law associated with thermodynamic force magnitude in the fibre direction
$m\ (-)$	Power coefficient of the quasi-static damage law associated with thermodynamic force in the transverse direction
$m_1\ (-)$	Power coefficient of the fatigue damage law associated with maximum thermodynamic force in the transverse direction
$m_2\ (-)$	Power coefficient of the fatigue damage law associated with thermodynamic force magnitude in the transverse direction
$n\ (-)$	Power coefficient of the quasi-static damage law associated with thermodynamic force in the shear direction
$n_1\ (-)$	Power coefficient of the fatigue damage law associated with thermodynamic force magnitude in the shear direction
$n_2\ (-)$	Power coefficient of the fatigue damage law associated with thermodynamic force magnitude in the transverse direction
$\tilde{p}\ (mm/mm)$	Cumulative effective plastic strain
$R_0\ (MPa)$	Hardening threshold according to kinematic hardening law
$V_f\ (\%)$	Fibre volume fraction of the composite specimen
$Y_A\ (MPa)$	Ultimate thermodynamic force in fibre direction when the matrix suffered no damage in a previous loading
$Y_B\ (MPa)$	Ultimate thermodynamic force in fibre direction when the matrix damage strongly reduced its contribution to the composite mechanical strength in fibre direction
$Y_{d_1}\ (MPa)$	Thermodynamic force related to the damage variable in the fibre direction
$Y_{d1}^{ult}\ (MPa)$	Ultimate thermodynamic force in the fibre direction
$Y_{d_2}\ (MPa)$	Thermodynamic force related to the damage variable in the transverse direction
$Y_{d_{12}}\ (MPa)$	Thermodynamic force related to the shear damage variable
$Y_0\ (MPa)$	Thermodynamic force related to the matrix damage threshold under quasi-static loading
$\alpha\ (-)$	Coupling parameter between transverse and shear loadings driving plastic strain
$\gamma\ (-)$	Power coefficient of the kinematic hardening law

$\gamma_1\ (-)$	Power coefficient of the fatigue damage law associated with pre-existing damage in fibre direction
$\gamma_2\ (-)$	Power coefficient of the fatigue damage law associated with pre-existing matrix damage
$\nu_{12}\ (-)$	Primary Poisson's ratio of the ply
$\nu_{21}\ (-)$	Secondary Poisson's ration of the ply
$\nu_f\ (-)$	Fibre Poisson's ratio
$\nu_m\ (-)$	Matrix Poisson's ratio
$\varepsilon_i\ (mm/mm)$	Strain in the fibre direction (i=1) or the transverse direction (i=2) at the ply scale, strain in the loading direction (i=xx) or in the transverse to loading direction (i=yy) at the laminate scale
$\gamma_{12}\ (mm/mm)$	Shear strain at the ply scale
$\varepsilon_2^e\ (mm/mm)$	Elastic strain in the transverse direction at the ply scale
$\gamma_{12}^e\ (mm/mm)$	Elastic shear strain at the ply scale
$\varepsilon_2^p\ (mm/mm)$	Plastic strain in the transverse direction at the ply scale
$\gamma_{12}^p\ (mm/mm)$	Plastic shear strain at the ply scale
$\tilde{\varepsilon}_2^p\ (mm/mm)$	Effective plastic strain in the transverse direction at the ply scale
$\tilde{\gamma}_{12}^p\ (mm/mm)$	Effective plastic shear strain at the ply scale
$\sigma_i\ (MPa)$	Stress in the fibre direction (i=1) or in the transverse direction (i=2) at the ply scale, stress in the loading direction (i=xx) or in the transverse to loading direction (i=yy) at the laminate scale
$\tau_{12}\ (MPa)$	Shear stress at the ply scale
$\tilde{\sigma}_2\ (MPa)$	Effective stress in the transverse direction at the ply scale
$\tilde{\tau}_{12}\ (MPa)$	Effective shear stress at the ply scale
X^0	Initial value of the mechanical property X

1 Introduction

The wind energy industry, like the transportation and marine industries, mostly uses thermoset-matrix composites to manufacture its products. However, these composite materials have limited recyclability. Thus, to reduce the environmental footprint, new polymer matrices have been developed in recent years to replace commonly used thermoset resins, including acrylic thermoplastic matrices. These have better recycling and repair opportunities, good fatigue and impact strengths and they are lighter. They also reduce manufacturing

costs since their polymerisation is performed at room temperature (RT) [1,2], resulting in a better production rate.

During its twenty years in service, a wind turbine blade (WTRB) undergoes 10^8 to 10^9 fatigue cycles [3,4] and is exposed to temperatures ranging from -20°C to +60°C. At the composite scale, these loadings can lead to a significant deterioration of the material mechanical properties, due to damage such as fibre-matrix debonding, cracking and delamination [5–8]. These different types of damage occur at different scales, they can interact with each other, and lead to premature fibre breakage [9,10]. Thus, the final fracture of the composite is due to a combination of these damage mechanisms [7]. Plus, for thermoplastic matrix composites, both the mechanical properties and the damage scenario can be impacted by temperature changes in a range far below the matrix glass transition temperature [11–18]. This has to be taken into account for purposes of designing wind turbine blades using acrylic-matrix composites as required by the French program EFFIWIND [19]. Even if some laboratory testing on some specific WTRB models showed damage occurrence in the composite material, namely delamination, fibre failure and crack propagation [20–26], most of the WTRBs end their operational lifetime without serious mechanical property degradation. Indeed, only between 5 and 20% of all WTRB incidents can be imputed to composite blade damage over the last decade as stated in [27–29]. One of the main reason is the WTRBS being greatly oversized due to the normative approach used by the certification bodies such as [30,31] for the prediction of the fatigue lifetime of their constitutive composite. Indeed, as stated in [32], the normative approach comes from the knowledge on metallic materials and is a macroscale approach, i.e. an approach at the laminate scale. Thus, predicting the fatigue behaviour of all the constitutive lamination in the WTRB leads to conservative assumptions which increase the gap between the model and the physical reality. The oversizing of WTRBs is a major issue when coming towards the design of longer blades (> 80m) as initiated by research institutes and industries [33–35] where mass is a critical issue. Therefore, it is crucial to develop more suitable damage models for WTRBs that can help reducing their weight.

Several damage models can be found in the literature [36–40] but they do not consider the temperature effect on the mechanical behaviour of composite materials. Models at the microscopic scale are promising but they cannot be used at the structure scale [41–43]. They focus instead on understanding phenomena and building or completing models at the mesoscale. A damage model at the mesoscale was already in use for the design of wind turbine blades as part of the EFFIWIND program [10,32]. It aimed at filling the lack of proper methods

for the prediction of the fatigue life of composite laminates [44], and thus, at reducing the oversizing of WTRBs. The purpose of the work presented in this paper was to determine if the validity domain of this damage model could be extended for a composite material with a temperature-dependent mechanical behaviour and damage scenario [16].

First, this paper describes the material under investigation and the effect of temperature on its mechanical behaviour under quasi-static tensile and fatigue loadings within the temperature range of wind turbine blades. Next, the damage model at the ply scale chosen to predict its mechanical behaviour under these two types of loadings is described. The model parameters are then identified at room temperature in order to validate the use of this damage model and finally, a simplified way of considering the effect of temperature on the composite mechanical behaviour in this model is proposed.

2 Material under investigation

2.1 Constituents and material health

The material under investigation is an amorphous acrylic-matrix and glass-fibre-reinforced laminate composite. The acrylic resin Elium™ 188 was supplied by ARKEMA and the G-Ply™ E-glass reinforcements were supplied by CHOMARAT. Two kinds of reinforcements were used, with their fibre sizing optimised to be combined with an acrylic resin: unidirectional plies UD960 CT3,8 (AC4), denoted "UD", and [±45] biaxial non-crimp fabrics (NCFs) BXS1000 C3,4 (AC4), denoted "BXS". Their main properties are summarised in Table 1 and their microstructure within the resin is shown in Figure 1. They highlight the fact that unidirectional plies have fibres in the weft direction nonetheless, and that biaxial NCFs [±45] have fibres in the warp direction. The laminate composite was produced by vacuum infusion at room temperature. During resin polymerisation, an exothermic reaction was observed, raising the panel temperature by 15°C to 25°C at its peak, which may lead to residual thermal stresses. The fibre fraction volume, denoted V_f and calculated from the reinforcement basis weight and the panel thickness, varies between 45% and 60%, and observations by optical microscope of coupons cut from the panels showed a porosity rate lower than 3%. The glass transition temperature of the Elium 188™ acrylic resin provided by the manufacturer is about 109°C, with a maximum service temperature fixed at 85°C.

Areal density	Unidirectional ply (UD [0])	Biaxial NCF (BXS [±45])
Ply weight (g/m²)	1007 ± 5%	1005 ± 5%
0° Warp weight (g/m²) – Glass	960 ± 5%	2 ± 5%
Weft weight (g/m²) - Glass	35 ± 5%	/
Diagonal 45° weight (g/m²) - Glass	/	500 ± 5%
Diagonal -45° weight (g/m²) - Glass	/	500 ± 5%
Tying weight (g/m²) - Polyester	12 ± 5%	3 ± 5%

Table 1: Properties from CHOMARAT technical datasheets of unidirectional plies and biaxial non-crimp fabrics used for the studied laminated composite

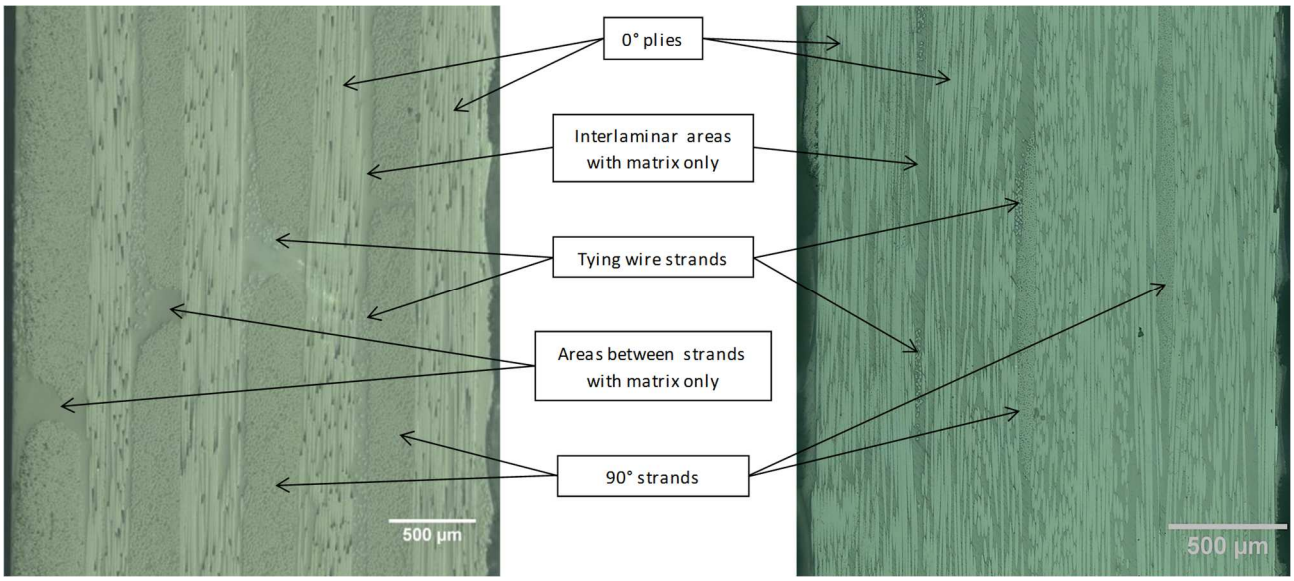

Figure 1: Microscopic images of BXS reinforcement (left) and UD reinforcement (right)

2.2 Effect of temperature on composite mechanical behaviour under quasi-static and fatigue loadings

First of all, as shown in Figure 2, at the ply scale, subscript "1" refers to the fibre direction, subscript "2" to the transverse direction to the fibres and subscript "12" to ply shear. At the laminate/specimen scale, subscript "x" refers to the loading direction, subscript "y" to the transverse direction to the loading direction and "xy" refers to laminate shear. Stresses, elastic modulus, and strains are referred to by, σ_i, E_i, ε_i respectively in fibre and transverse directions, and by τ_{ij}, G_{ij} and $\gamma_{ij} = 2 * \varepsilon_{ij}$ under shear loadings. ν_{12} and ν_{21} refer to the ply primary and secondary Poisson's ratios respectively.

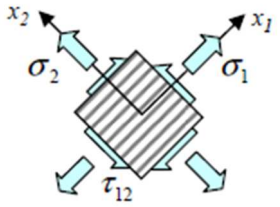

Figure 2: Ply spatial reference [32]

Testing temperatures were taken from within the temperature service range of wind turbine blades, i.e. between -20 and +60°C. Previous tensile tests with in-situ observations clearly showed a change in the damage scenario between 15 and 40°C [15,16,45], so mechanical tests were mainly performed at both these temperatures, in addition to RT (20°C). Mechanical tests on BXS $[(\pm 45)_2]_s$ specimens were performed at 1, 15, RT, 30 and 48°C. For quasi-static tensile tests in the fibre direction, BXS $[(0/90)_2]_s$ standard specimens were used instead of UD $[0]_4$ standard specimens (Figure 3(a)), as their final rupture occurred in the gage length unlike UD $[0]_4$ specimens which consistently broke in their tabs. Under fatigue loadings, dogbone specimens were used to ease a final rupture within the gage length, as proposed by De Baere et al. [46] (Figure 3(b)). However, the used UD $[0]_4$ specimens still broke in their tabs due to interlaminar delamination caused by a manufacturing defect, i.e. a slight misorientation of one or more of the 0° plies against the loading direction, causing significant experimental scattering and thus preventing a proper assessment of the temperature effect. Thus, BXS $[(0/90)_2]_s$ dogbone specimens were used instead as their final rupture occurred consistently within the gage length, leading to poorly scattered results (see Figure 4(b)). Tensile tests were performed at 0.5mm/min and fatigue tests at a load ratio $R = 0.1$. Either a biaxial strain gauge or both longitudinal and transverse extensometers were used to measure specimen longitudinal and transverse strains.

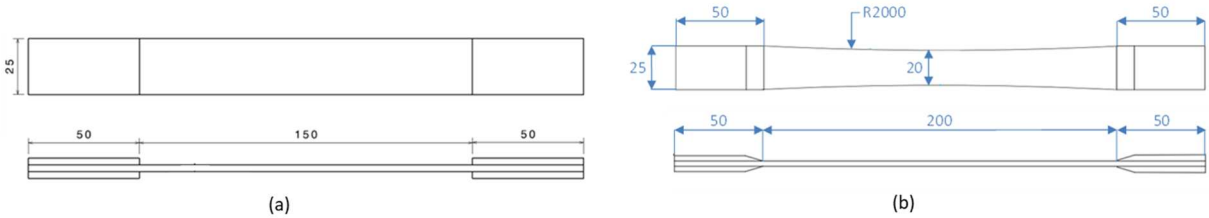

Figure 3: Specimen geometry: (a) coupons for mechanical tests in an off-axis direction and (b) dogbone specimens for mechanical tests in the fibre direction – thickness between 3-6mm and 5-10mm without and with tabs, respectively

Tensile and fatigue tests performed in the composite fibre direction showed a poorly temperature-dependent mechanical behaviour between 15 and 40°C, which is consistent with the literature [14,47] (Figure 4). However, quasi-static tensile and fatigue tests performed in the ply off-axis direction showed a significant effect of temperature, as shown in Figure 5 for BXS $[(\pm 45)_2]_s$ specimens. The results are shown at the ply scale.

Indeed, for this lamination, shear stress and strain at the ply scale, τ_{12} and γ_{12}, can be easily obtained from the specimen stress and longitudinal and transverse strains, σ_{xx}, ε_{xx} and ε_{yy}, respectively, using the following stress and strain transformation equations [48]:

$$\tau_{12} = \frac{\sigma_{xx}}{2} \quad (1)$$

$$\gamma_{12} = \varepsilon_{xx} - \varepsilon_{yy} \quad (2)$$

For this lamination, the stress level at a given shear elastic strain clearly decreases as the temperature increases from 1 to 48°C under a quasi-static tensile loading, while under a fatigue loading with a load ratio R=0.1, fatigue strength is around half a decade lower as the temperature increases from 15 to 40°C. These trends are consistent with those found in the literature [12–14]. This is also consistent with the results of the studies by Cadieu et al. [17,18] on a similar composite material, enhanced for impact resistance.

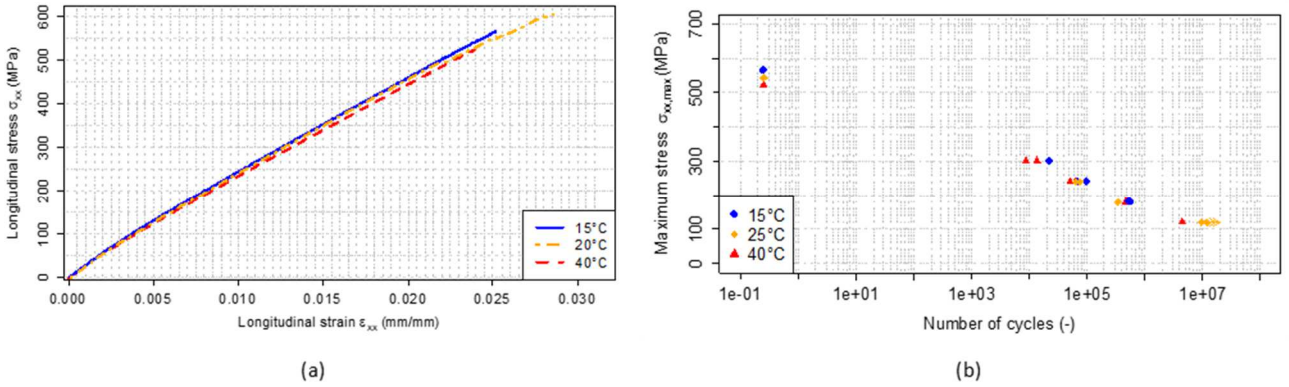

Figure 4: Effect of temperature on the composite mechanical behaviour in the fibre direction under (a) tensile loading, (b) fatigue loading at $R = 0.1$ – BXS $[(0/90)_2]_s$ specimens – results at the laminate scale

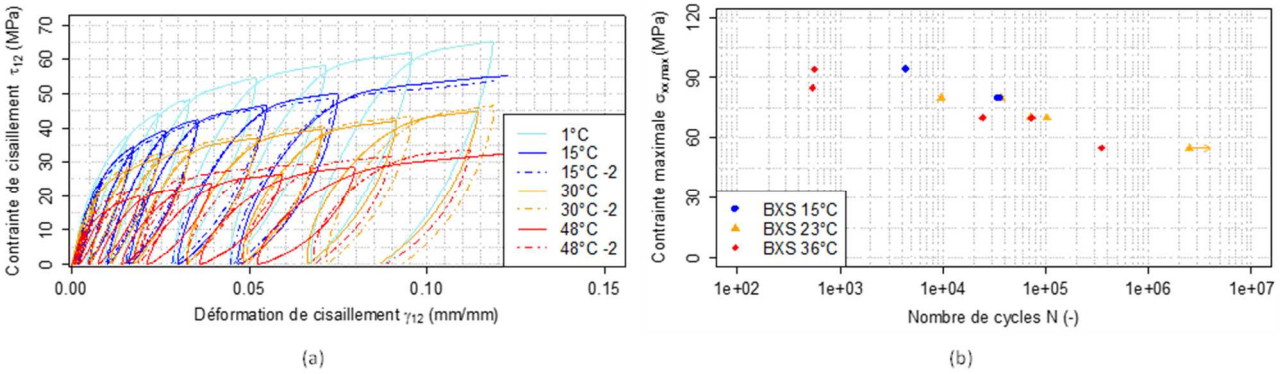

Figure 5: Effect of temperature on the composite off-axis mechanical behaviour under (a) tensile loading, (b) fatigue loading at $R = 0.1$ - BXS $[(\pm 45)_2]_s$ specimens – results at the ply scale

3 Damage model

The damage model originates from Ladevèze et al. [38] and was further developed by several studies [10,32,36,49–51,37,52]. It is based on damage mechanics and is formulated at the ply scale, with plies regarded as homogeneous orthotropic [52]. Three internal variables are used to describe the stiffness loss of the ply: one describing the brittle failure of fibres under a load in the fibre direction, d_1, one describing the ply stiffness loss in the fibre transverse direction, d_2, and one describing the shear stiffness loss of the ply, d_{12}. Under a tensile load, only the in-plane transversal and shear moduli are modified, under the assumption of progressive damage associated with micro-cracks and fibre matrix decohesion parallel to the fibres [37]. A plastic-hardening model coupled to damage describes the inelastic strains.

Assuming plane stresses and small perturbations, the elastic strain energy of a ply can be written in the following form:

$$E_D = \frac{1}{2}\left[\frac{\sigma_1^2}{E_1^0(1-d_1)} + \frac{\langle\sigma_2\rangle_+^2}{E_2^0(1-d_2)} + \frac{\langle\sigma_2\rangle_-^2}{E_2^0} - 2\frac{\nu_{12}^0\sigma_1\sigma_2}{E_1^0} + \frac{\tau_{12}^0}{G_{12}^0(1-d_{12})}\right] \tag{3}$$

where $\langle . \rangle_+$ is the positive part and $.^0$ refers to the initial value (i.e. before any damage in the composite). The tension energy and compression energy in the transverse direction of fibres are split in order to describe the unilateral feature due to the opening and closing of the micro-defects [53]. A thermodynamic force can be associated to each damage variable by considering the respective elastic strain energy derivatives:

$$\begin{cases} Y_{d1} = \dfrac{\partial E_D}{\partial d_1} = \dfrac{\sigma_1^2}{2E_1^0(1-d_1)^2} \\ Y_{d2} = \dfrac{\partial E_D}{\partial d_2} = \dfrac{\sigma_2^2}{2E_2^0(1-d_2)^2} \\ Y_{d12} = \dfrac{\partial E_D}{\partial d_{12}} = \dfrac{\tau_{12}^2}{2G_{12}^0(1-d_{12})^2} \end{cases} \tag{4}$$

Damage described by the internal variables d_1, d_2 and d_{12} can be due to a monotonic loading as well as a fatigue loading [36], which for the laminated composite under investigation leads to similar damage mechanisms, given the experimental data and data from the literature [15,16,45]. Thus, the model considers that these two damage sources are cumulative. Furthermore, as the cracks are perpendicular to the fibres and their impact on the transverse and shear loss of stiffness is similar, internal damage variables d_2 and d_{12} are

taken as proportional to each other, as proposed by Ladevèze et al. [38] and Hochard et al. [52]. These two assumptions translate into the following relations:

$$\begin{cases} d_1 = d_1^s + d_1^f \\ d_2 = d_2^s + d_2^f \\ d_{12} = c d_2 \end{cases} \tag{5}$$

where superscript *s* refers to quasi-static loading, and superscript *f* refers to fatigue loading.

Damage variables can also be expressed as a function of the ply moduli, as follows:

$$\begin{cases} d_1 = 1 - \dfrac{E_1}{E_1^0} \\ d_2 = 1 - \dfrac{E_2}{E_2^0} \\ d_{12} = 1 - \dfrac{G_{12}}{G_{12}^0} \end{cases} \tag{6}$$

3.1 Under quasi-static loadings

- *Modelling damage evolution*

The brittle failure of fibres under a tensile loading in the fibre direction is described as follows:

$$\begin{cases} d_1 = d_1^s = 0 \; if \; Y_{d_1} < Y_{d_1}^{ult}(d_2) \\ d_1 = d_1^s + d_1^f = 1 \; if \; Y_{d_1} > Y_{d_1}^{ult}(d_2) \end{cases} \tag{7}$$

where $Y_{d_1}^{ult}$ is the thermodynamic force associated to the ply ultimate strength in the fibre direction, which depends on the matrix damage state. Several authors have shown that the presence of damage in the matrix decreases the ply ultimate strength in the fibre direction [10,52]. This decrease can be described by the following law, proposed by Caous et al. [10,32] :

$$Y_{d1}^{ult}(d_2) = \frac{Y_A - Y_B}{1 + e^{(d_2 - d_m)/d_\lambda}} + Y_B \tag{8}$$

where Y_A, Y_B, d_m and d_λ are parameters to identify experimentally, which depend on the composite material under investigation. Parameter Y_A is the thermodynamic force associated with the ultimate strength of fibres aligned with the loading direction when the matrix suffered no damage in a previous loading ($d_2 = 0$) and parameter Y_B is the thermodynamic force associated with the ultimate strength when the matrix is so damaged from previous loadings that its contribution to the composite mechanical strength is strongly reduced.

Parameters d_m and d_λ are considered independent from the reinforcement type and from the fibre fraction volume, contrary to Y_A and Y_B which are corrected to the latter [10,32].

Regarding the matrix damage, several evolution laws have been proposed in the literature [36,38,49,52]. That proposed by Hochard et al. [52] has been chosen here due to its ability to describe satisfactorily the mechanical behaviour of thermoset laminated composites reinforced with glass fibres [32,52]:

$$d_2^s = \langle 1 - e^{-(a(Y_{d2})^m + b(Y_{d12})^n - Y_0)} \rangle_+ \tag{9}$$

where a, m, b, n and Y_0 are parameters to identify experimentally, which depend on the composite material under investigation. Y_0 matches the threshold value of the development of d_2^s.

- *Modelling plastic strain evolution*

Stress-strain curves in off-axis directions highlight residual strains when samples are unloaded. These residual strains are not only due to plasticity in the polymer matrix but also to sliding between micro-crack lips or fibre matrix decohesion, justifying the presence of hysteresis loops in $[(\pm 45)_2]_s$ specimens. Viscous phenomena can also participate in this complex response. In the model, for simplicity, a plasticity model is used to represent residual strains. The total strains in off-axis directions are then divided into an elastic part and a plastic part, as follows:

$$\varepsilon_2 = \varepsilon_2^e + \varepsilon_2^p \tag{10}$$

$$\gamma_{12} = \gamma_{12}^e + \gamma_{12}^p \tag{11}$$

where exponents *e* and *p* refer to the elastic and the plastic parts, respectively.

The coupling of damage and plasticity is taken into account by using effective stress and effective strain [32,37,38,50], which are defined as:

$$\tilde{\sigma}_2 = \frac{\sigma_2}{1 - d_2} \;\; and \;\; \dot{\tilde{\varepsilon}}_2^{\,p} = \dot{\varepsilon}_2^p \, (1 - d_2) \;\; si \;\; \sigma_2 > 0 \tag{12}$$

$$\tilde{\sigma}_2 = \sigma_2 \;\; and \;\; \dot{\tilde{\varepsilon}}_2^{\,p} = \dot{\varepsilon}_2^p \;\; si \;\; \sigma_2 < 0 \tag{13}$$

$$\tilde{\tau}_{12} = \frac{\tau_{12}}{1 - d_{12}} \;\; and \;\; \dot{\tilde{\gamma}}_{12}^p = \dot{\gamma}_{12}^p (1 - d_{12}) \tag{14}$$

The hardening function driving the plastic strain evolution is defined as:

$$f = \sqrt{\tilde{\tau}_{12}^2 + \alpha^2 \tilde{\sigma}_2^2} - K\,\tilde{p}^{\gamma} - R_0 \; with \; f \leq 0 \tag{15}$$

where α, K, γ and R_0 are parameters to be identified experimentally, which depend on the composite material under investigation. $\tilde{p}$ is the fourth internal variable of the model, matching the cumulative effective plastic strain. R_0 refers to the initial plastic strain threshold.

If $f < 0$, $\dot{\tilde{p}} = 0$. Otherwise, the plastic flow rules give:

$$\begin{cases} \dot{\tilde{\varepsilon}}_2^p = \dfrac{\alpha^2\,\tilde{\sigma}_2}{K\,\tilde{p}^{\gamma} + R_0}\dot{\tilde{p}} \\ \dot{\tilde{\gamma}}_{12}^p = \dfrac{\tilde{\tau}_{12}}{K\,\tilde{p}^{\gamma} + R_0}\dot{\tilde{p}} \end{cases} \tag{16}$$

3.2 Under fatigue loadings

As proposed by Hochard et al. and Caous [32,37], regarding fatigue loadings, damage evolution depends on both the maximum loading and the loading amplitude. Evolution laws are written as:

$$\begin{cases} \dfrac{\partial d_1^f}{\partial N} = a_1(1-d_1)^{\gamma_1}\left(Y_{d_1^f}\right)^{l_1}\left(\Delta Y_{d_1^f}\right)^{l_2} \\ \dfrac{\partial d_2^f}{\partial N} = (1-d_2)^{\gamma_2}\left(a_2\left(Y_{d_2^f}\right)^{m_1}\left(\Delta Y_{d_2^f}\right)^{m_2} + b_2\left(Y_{d_{12}^f}\right)^{n_1}\left(\Delta Y_{d_{12}^f}\right)^{n_2}\right) \end{cases} \tag{17}$$

where a_1, a_2, b_2, γ_1 , γ_2, l_1, l_2, m_1, m_2, n_1 and n_2 are parameters to be identified experimentally, which depend on the composite material under investigation, N is the number of load cycles, and $Y_{d_i^f}$ and $\Delta Y_{d_i^f}$ refer to the thermodynamic forces associated with the maximum stress of the fatigue loading and the loading amplitude, respectively, defined as follows:

$$\begin{cases} Y_{d_1^f} = \dfrac{\sigma_{1\,max}^2}{2E_1^0(1-d_1)^2} \\ Y_{d_2^f} = \dfrac{\langle\sigma_{2\,max}\rangle_+^2}{2E_2^0(1-d_2)^2} \\ Y_{d_{12}^f} = \dfrac{\tau_{12\,max}^2}{2G_{12}^0(1-d_{12})^2} \end{cases} \quad and \quad \begin{cases} \Delta Y_{d_1^f} = \dfrac{(\sigma_{1\,max} - \sigma_{1min})^2}{2E_1^0(1-d_1)^2} \\ \Delta Y_{d_2^f} = \dfrac{(\langle\sigma_{2\,max}\rangle_+ - \langle\sigma_{2\,min}\rangle_+)^2}{2E_2^0(1-d_2)^2} \\ \Delta Y_{d_{12}^f} = \dfrac{(\tau_{12\,max} - \tau_{12\,min})^2}{2G_{12}^0(1-d_{12})^2} \end{cases} \tag{18}$$

It is worth noting that fatigue loadings do not generate an increase in plastic strain directly, but the evolution of fatigue damage variables d_2^f and d_{12}^f will increase the plastic strain indirectly since the hardening law is defined using the effective stresses. Evolution laws in the transverse and shear directions were developed to model a gradual stiffness loss in these directions, as observed experimentally. The evolution law in the fibre

direction also models a gradual stiffness loss in this direction, whereas none is observed experimentally. This stiffness loss has to be introduced so that the model is able to assess the composite lifetime in the fibre direction, whatever the applied maximum stress [10,32]. Introducing a relation between the failure threshold in the fibre direction and the matrix damage, like under a quasi-static loading, will not be a solution since the ultimate strength for maximum matrix damage may still be around several hundreds of MPa (512MPa for the composite tested in [10,32]).

4 Identification of the model parameters at room temperature

4.1 Identification of the initial elastic properties of the ply

All experimental tests were performed at room temperature, i.e. 20°C. The ply initial elastic modulus in the fibre direction E_1^0 and the primary Poisson's ratio ν_{12}^0 were obtained from tensile tests on UD $[0]_4$ specimens, with a fibre fraction volume V_f varying between 53% and 59%. The ply initial transverse elastic modulus and the secondary Poisson's ratio were obtained from tensile tests on UD $[90]_4$ specimens with V_f varying between 56% and 59%. Finally, the ply initial shear elastic modulus was obtained from tensile tests on UD and BXS $[(\pm 45)_2]_s$ specimens, with V_f varying between 50% and 57%. Thus, the initial elastic properties of the ply are not obtained at the same fibre fraction volume. To overcome this issue and thus to take into account the variation of fibre fraction volume, values obtained experimentally were adjusted using modified mixture laws derived from the mixture laws for composites given below [54]:

$$\begin{cases} E_1^0 = V_f E_f^0 + E_m^0(1-V_f) \approx V_f E_f^0 \; with \; E_m^0 \ll E_f^0 \\ \nu_{12}^0 = \nu_f^0 V_f + \nu_m^0(1-V_f) \\ E_2^0 = E_m^0 \left(\dfrac{1}{(1-V_f) + \dfrac{E_m^0}{E_{ft}^0} V_f} \right) \approx \dfrac{E_m^0}{1-V_f} \; with \; E_m^0 \ll E_{ft}^0 \\ \nu_{21}^0 = E_2^0 \dfrac{\nu_{12}^0}{E_1^0} \\ G_{12}^0 = \dfrac{G_m^0}{(1-V_f) + \dfrac{G_m^0}{G_f^0} V_f} \approx \dfrac{G_m^0}{1-V_f} with \; G_m^0 \ll G_f^0 \end{cases} \tag{19}$$

where $E_{\cdot}^0$ refers to the initial elastic modulus, $\nu_{\cdot}^0$ to the initial Poisson's ratio and $G_{\cdot}^0$ to the initial shear elastic modulus with the subscripts "m", "f" and "ft" denoting a matrix property, a fibre property in the fibre direction and a fibre property in the fibre transverse direction, respectively. Considering that E_m^0 and G_m^0 are

usually much lower respectively than both E_f^0 and E_{ft}^0 and G_f^0, these mixture laws were simplified, as shown in Equation (19). In order to take into account the fact that a UD ply is only 95% unidirectional as 5% of its fibres are in its transverse direction, these mixture laws were then modified using equations for composites with woven fabrics from [54], as shown below:

$$\begin{cases} E_1^0 = 0.95 * V_f E_f^0 + 0.05 * \dfrac{E_m^0}{1 - V_f} \approx 0.95 * V_f E_f^0 \; with \; E_m^0 \ll E_f^0 \\ \nu_{12}^0 = \dfrac{\nu_f^0 V_f + \nu_m^0 (1 - V_f)}{0.95 + 0.05 * \dfrac{V_f E_f^0}{E_m^0/(1 - V_f)}} \\ E_2^0 = 0.95 * \dfrac{E_m^0}{1 - V_f} + 0.05 * V_f E_f^0 \\ \nu_{21}^0 = E_2^0 \dfrac{\nu_{12}^0}{E_1^0} \\ G_{12}^0 = \dfrac{G_m^0}{(1 - V_f)} \end{cases} \tag{20}$$

E_m^0, E_f^0, ν_f^0, ν_m^0 and G_m^0 were identified with an Ordinary Least Squares (OLS) regression, as proposed by Caous et al. [32], except for ν_f^0. As numerous value combinations can be found for ν_f^0 and ν_m^0, the value of ν_m^0 was taken from the literature [54] and thus was considered to be equal to 0.25 and an OLS regression was used to obtain ν_f^0. Identified values are given in Table 2. Accordingly, the mechanical properties given as inputs for the model are the values identified for the matrix and fibre initial elastic properties and the fibre fraction volume V_f instead of the initial mechanical properties of the ply. As it will be seen later in part 5 of this paper, this is a relevant point in order to consider the temperature effect on the composite off-axis mechanical behaviour in the model in a concise way. It is worth noting that the relationship linking the initial shear modulus to the initial Young modulus and Poisson's ratio for isotropic homogeneous materials defined below gives $G_m^0 = 2{,}0 \; GPa$. This means that this relationship is well respected.

$$G_m^0 = \frac{E_m^0}{2(1 + \nu_m^0)} \tag{21}$$

$E_f^0 \; (GPa)$	$\nu_f^0 \; (-)$	$E_m^0 \; (GPa)$	$G_m^0 \; (GPa)$	$\nu_m^0 \; (-)$
74	0.29	5.5	2.1	0.33(*)

Table 2: Identified values of the fibre and matrix elastic properties at 20°C – (*) value taken from the literature, [54], for a physically consistent value for ν_f^0

4.2 Identification of the parameters of the damage evolution laws under a quasi-static loading

- *Identification method*

Parameters d_λ and d_m of the damage evolution law in the fibre direction (Equation (8)) were taken as equal to the values identified in [10,32], as the reinforcements under investigation are similar. Parameters Y_{Af} and Y_{Bf} were identified using an OLS regression from quasi-static tensile tests performed on BXS $[(0/90)_2]_s$ specimens at room temperature (Figure 4(a)), but also at 110°C. At this temperature, the matrix contribution to specimen mechanical strength is strongly reduced and should reach a minimum value which agrees with that obtained with a high level of damage [10,32]. BXS $[(0/90)_2]_s$ specimens were used instead of UD $[0]_4$ specimens for the reasons given in section 2.2.

Parameters of the matrix damage evolution law (Equation (9)) were identified from quasi-static tensile tests performed at room temperature on $[(\pm45)_2]_s$ specimens for both reinforcements and on $[90]_4$ specimens for the UD reinforcement. In such laminates, the loading mainly causes shear stress and transverse stress at the ply scale. This means that the contribution of the transverse damage and the shear damage to the total matrix damage can be disregarded for tests performed on $[(\pm45)_2]_s$ and $[90]_4$ specimens respectively. Accordingly, the evolution laws (Equations (9) and (15)) can be simplified, as shown below for $[(\pm45)_2]_s$ laminates:

$$d_{12}^s = \langle 1 - e^{-(b(Y_{d12})^n - Y_0)} \rangle_+ \tag{22}$$

$$\tilde{\tau}_{12} = K\, \dot{\tilde{\gamma}}_{12}^{p\,\gamma} + R_0 \tag{23}$$

and as shown below for $[90]_4$ laminates:

$$d_2^s = \langle 1 - e^{-(a(Y_{d2})^m - Y_0)} \rangle_+ \tag{24}$$

$$\tilde{\sigma}_2 = \frac{1}{\alpha}\left(K \left(\frac{\dot{\tilde{\varepsilon}}_2^p}{\alpha} \right)^\gamma + R_0 \right) \tag{25}$$

Thus, the identification of the matrix damage law parameters is uncoupled between the parameters concerning the contribution of the shear damage on the one hand, i.e. b, n, Y_0, K, γ and R_0, and those concerning the contribution of the transverse damage on the other hand, i.e. a, m, and α. n is taken as equal to 0.5. In this

way, the mechanical behaviour of the specimen can be satisfactorily described up to a shear strain of around 4%. Indeed, real-life structure loadings do not exceed this strain level.

First, b and Y_0 are identified by plotting d_{12}^s against Y_{d12} (Figure 6(a)) and K, γ and R_0 by plotting $\tilde{\tau}_{12}$ against $\dot{\tilde{\gamma}}_{12}^p$ (Figure 6(b)). These quantities are determined from the experimental data of UD and BXS $[(\pm45)_2]_s$ specimens using Equations (6) and (14). Next, a and m are identified by plotting d_2^s against Y_{d2} and α by plotting $\tilde{\sigma}_2$ against $\dot{\tilde{\varepsilon}}_2^p$. These quantities are also determined from the experimental data, using Equations (6) and (12). In this work, this identification process was performed through OLS regressions. Lastly, values of a, m, and α for the BXS reinforcement were taken as equal to the mean values identified for the UD reinforcement. All the parameter mean values can be seen in Table 3.

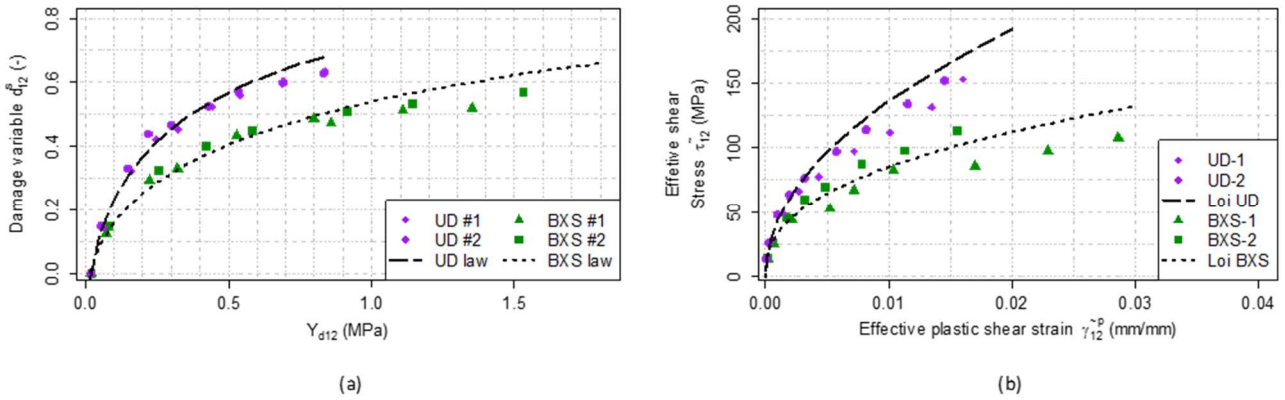

Figure 6: Identification of the parameters of the matrix damage evolution law from the experimental results of the quasi-static tensile tests performed at 0.5mm/min on UD and BXS $[(\pm45)_2]_s$ specimens with (a) d_{12}^s against Y_{d12} and (b) $\tilde{\tau}_{12}$ against $\dot{\tilde{\gamma}}_{12}^p$

Parameters	Test specimens	UD reinforcement	BXS reinforcement
$Y_{Af}\ (MPa)$	BXS $[(0/90)_2]_s$	32.9 ± 6.5	cf. UD value
$Y_{Bf}\ (MPa)$	BXS $[(0/90)_2]_s$	8.2 ± 1.3	cf. UD value
$d_m\ (-)$	Taken from [10]	0.49	cf. UD value
$d_\lambda\ (-)$	Taken from [10]	0.0035	cf. UD value
$n\ (-)$	Hypothesis	0.50	0.50
c $(-)$	Hypothesis	1	1
$b\ (MPa^{-m})$	$[(\pm45)_2]_s$ specimens (V_f = 50.5 ± 0.1% - BXS; 56.5 ± 0.1% - UD)	1.46 ± 0.04	0.88 ± 0.00
$Y_0\ (-)$		0.20 ± 0.01	0.10 ± 0.00
$K(MPa)$		1015 ± 389	542 ± 134
$\gamma\ (-)$		0.46 ± 0.03	0.40 ± 0.02

$R_0(MPa)$		0.00 ± 0.00	0.00 ± 0.00
$a\ (MPa^{-m})$	$[90]_4$ (V_f = 57.7 ± 0.2%)	2.47 ± 1.62	cf. UD value
$m\ (-)$		0.81 ± 0.26	cf. UD value
$\alpha\ (-)$		0.86 ± 0.13	cf. UD value

Table 3: Identified mean values for parameters of the evolution laws under a quasi-static loading (Equations (8), (9) and (15)) through OLS regressions – except for values of a, m and α for BXS reinforcement, which were taken as equal to those identified for the UD reinforcement and for d_m and d_λ which were taken as equal to those identified in [10]

- *Model validation*

Values identified for the model parameters were used to predict the mechanical behaviour of several laminations, some of which were not used for the identification procedure. Comparisons between model predictions and experimental data are shown in Figure 7 for laminations with plies in the loading direction and in Figure 8 for off-axis and transverse laminations.

These comparisons show that the composite mechanical behaviour in the fibre direction is well predicted. The difference between the model and the experimental ultimate strength for UD $[0]_4$ lamination is directly linked to the fact that the identification is done on BXS $[(0/90)_2]_s$ specimens, which show a greater ultimate strength with their failure occurring in the gage length, while UD $[0]_4$ specimens break prematurely in the tabs. The modelled ultimate strength for UD $[0/90_3/0]$ lamination cannot be compared to the experimental data since all tensile tests were ended before the specimen broke. This choice was made in order to then be able to observe damage to specimen edges by successive polishings, as described in [16]. Finally, experimental data show that the UD $[0]_4$ specimens exhibit progressive damage before their final failure. This phenomenon is attributed to the dogbone shape of the specimens.

Figure 8(a) shows that the model prediction for the mechanical behaviour of BXS $[(\pm45)_2]_s$ lamination is satisfactory. For UD $[(+45/-45)_2]_s$ and UD $[(+60/-60)_2]_s$ laminations (respectively Figure 8(c) and Figure 8(d)), the model overestimates their damage evolution. Indeed, the stress softening caused by damage and plasticity occurrence is stronger than the experimental one. Conversely, the model slightly underestimates the damage level for UD $[90]_4$ lamination (Figure 8(b)). These results may imply that the parameter identification should be improved or that the chosen damage model is not perfectly adapted. This will be discussed in Section 5. However, it must be kept in mind that in practice, the shear and transverse strain in each composite ply in a

structure such as a wind turbine blade will not exceed 1 and 0.5% respectively. Below these thresholds, the model gives a satisfactory prediction.

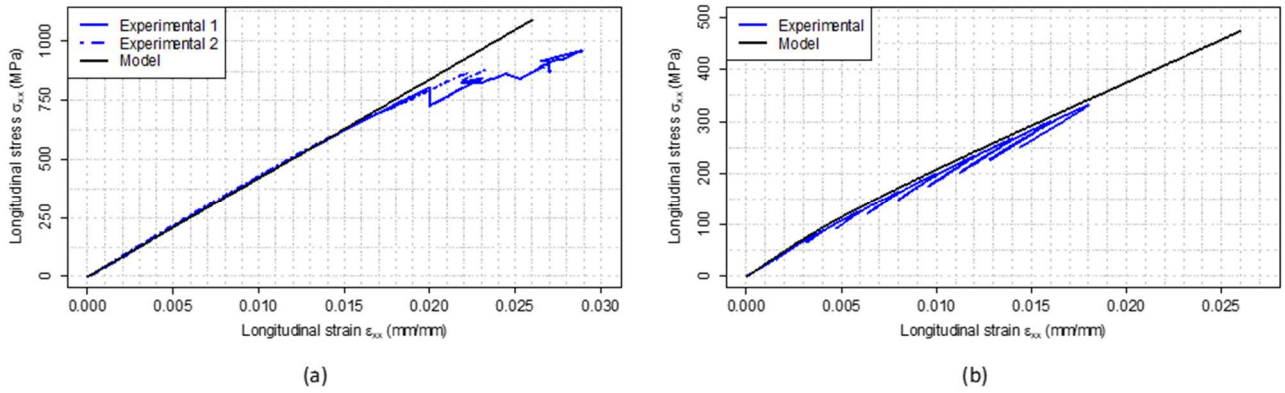

Figure 7: Comparison of model predictions and experimental data for a tensile loading applied to (a) UD $[0]_4$ with $V_f = 56{,}7\%$ and (b) UD $[0/90_3/0]$ with $V_f = 57.3\%$ (all tensile tests ended before specimen breakage)

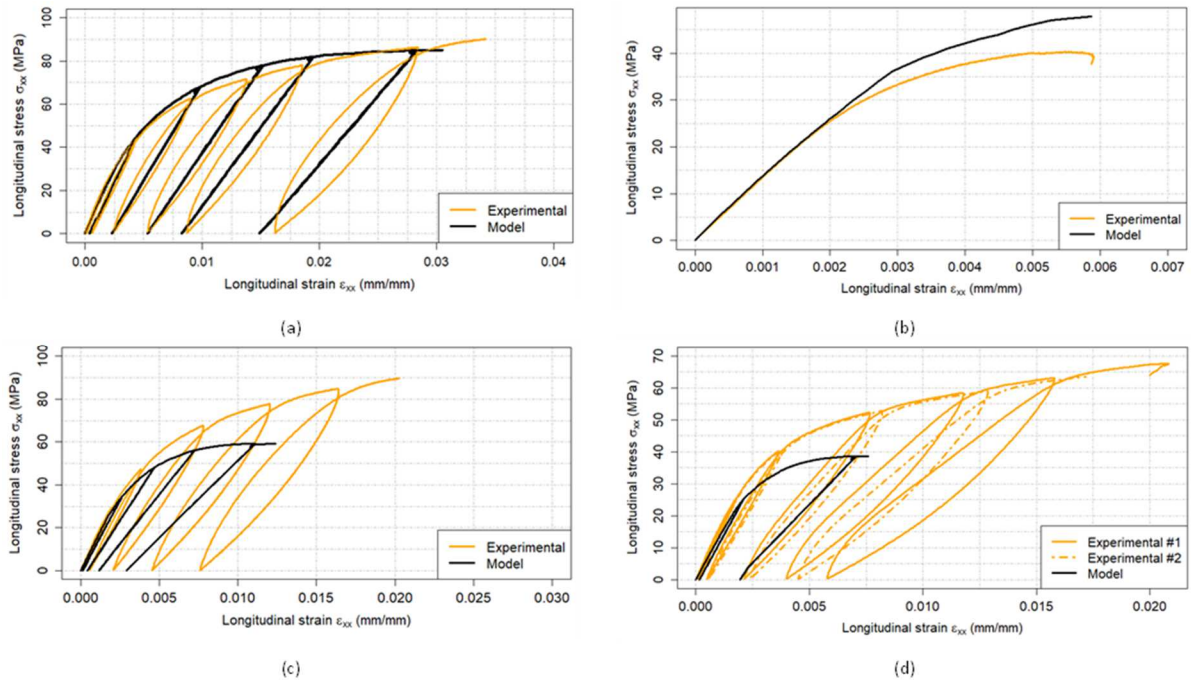

Figure 8: Comparison of model predictions and experimental data for a tensile loading applied to (a) BXS $[(\pm 45)_2]_s$ with $V_f = 50.5\%$, (b) UD $[90]_4$ with $V_f = 57.7\%$, (c) UD $[(+45/-45)_2]_s$ with $V_f = 56.2\%$ and (d) UD$[(+60/-60)_2]_s$ with $V_f = 58.1\%$

4.3 Identification of the parameters of the damage evolution laws under a fatigue loading

Parameters of the damage evolution laws (cf. Equations (17)) were identified using Poincaré's Balayage Method which consists in scanning the values that they can take. The set of parameters giving the best correlation between the model prediction and the experimental fatigue strength and damage evolutions was then selected. Experimental data came from fatigue tests performed at $R = 0.1$ (tensile-tensile load) and $R = -1$ (tensile-compressive load). These values were chosen as their R-ratios in both tensile-tensile and compression-tensile configurations are sufficiently distant one from another to distinguish the effect of the

maximum loading and the effect of the loading amplitude, while matching R-ratios that wind turbine blades undergo, as show in Figure 9 [32,55]. In particular, fatigue tests at the selected R-ratios are required by the wind turbine blade certification body Germanisher-Lloyd [31]. The fatigue tests were performed on UD $[0]_4$ dogbone specimens for the damage evolution law in the fibre direction and on BXS $[(\pm 45)_2]_s$ coupons for the matrix damage evolution law. If some UD $[0]_4$ specimens broke in their tabs due to the manufacturing defect described in Section 2.2, especially for high stress levels, most of them broke due to sparse fibre raveling within the gage area, making the S-N experimental points usable. Experimental results, presented in Figure 11 and Figure 12, highlight the fact that the influence of load ratio is important in both laminate sequences. These results also demonstrate the effect of mean stress. For instance, for UD $[0]_4$ specimens, with the same maximal stress of 250 MPa, a mean stress of zero ($R = -1$) gives a fatigue life of around 2.10^4 cycles while a mean stress of 137.5 MPa ($R = 0.1$) gives a fatigue life of around 2.10^6 cycles.

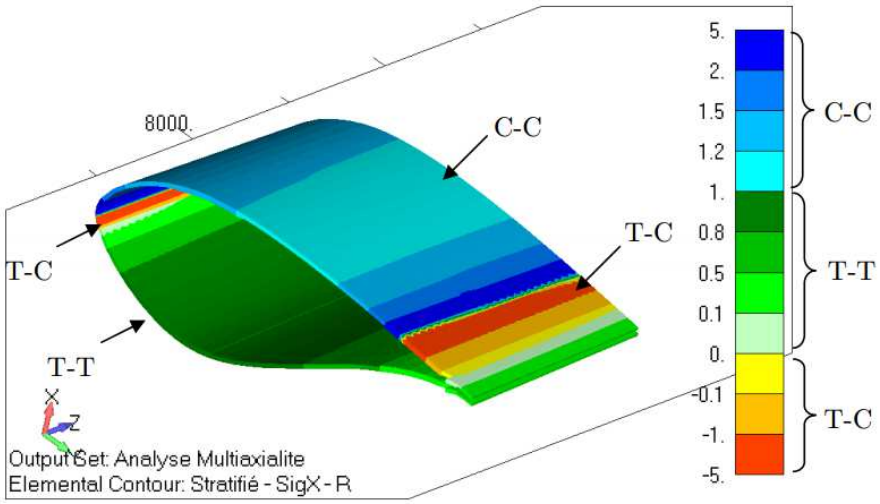

Figure 9: R-ratios commonly observed in wind turbine blades (C-C : Compression-Compression R-ratios; T-T : Tensile-Tensile R-ratios; T-C: Tensile-Compression R-ratios) [32]

As stated before for a quasi-static loading, axial loading on $[(\pm 45)_2]_s$ laminates mainly generates shear stresses. Accordingly, the contribution of the transverse damage to the total matrix can be disregarded. Equation (17) can then be simplified as follows:

$$\frac{\partial d_{12}^f}{\partial N} = b_2(1-d_{12})^{\gamma_2}\left(Y_{d_{12}^f}\right)^{n_1}\left(\Delta Y_{d_{12}^f}\right)^{n_2} \tag{26}$$

The fatigue tests at $R = -1$ were performed using an anti-buckling device designed for the specimen geometry used in this study based on the design proposed by E. Boyum [56] (Figure 10(a)). This device was used as it is able to prevent specimen buckling while limiting friction and its consequences. It is composed of two upper parts and two lower parts which are displaceable in relation to one another, depending on the specimen strain.

Thus, friction issues are not significant and do not impact fatigue test results, as shown in several studies [57–59]. The anti-buckling device used here was designed in such a way that there is a small clearance between its upper parts and the specimen gauge section on both sides to reduce the confinement of the specimen and reduce friction. In addition, in order to prevent friction even more efficiently, PTFE films were set between the test specimens and the device (Figure 10(b)), which was also designed with a thermocouple groove on one side (cf. Figure 10(a) & (b)) so that the increase in specimen temperature could be monitored. However, as soon as the specimen critical buckling force is reached, buckling is observed in the sliding area of the upper and lower parts of the anti-buckling device. To overcome this, a "U" shaped part was added at the level of the sliding area (Figure 10(b)). At $R = 0.1$, a fatigue loading in the fibre direction without the anti-bucking device leads to a small rise in the temperature of the specimen, of up to 2°C depending on the stress level. For fatigue tests on BXS $[(\pm 45)_2]_s$ coupons, the loading frequency was chosen in order to achieve a maximum specimen temperature increase of 5°C. In both cases, at the same loading frequencies, similar temperature increases were observed at $R = -1$, confirming the absence of significant friction between the specimen and the anti-buckling device.

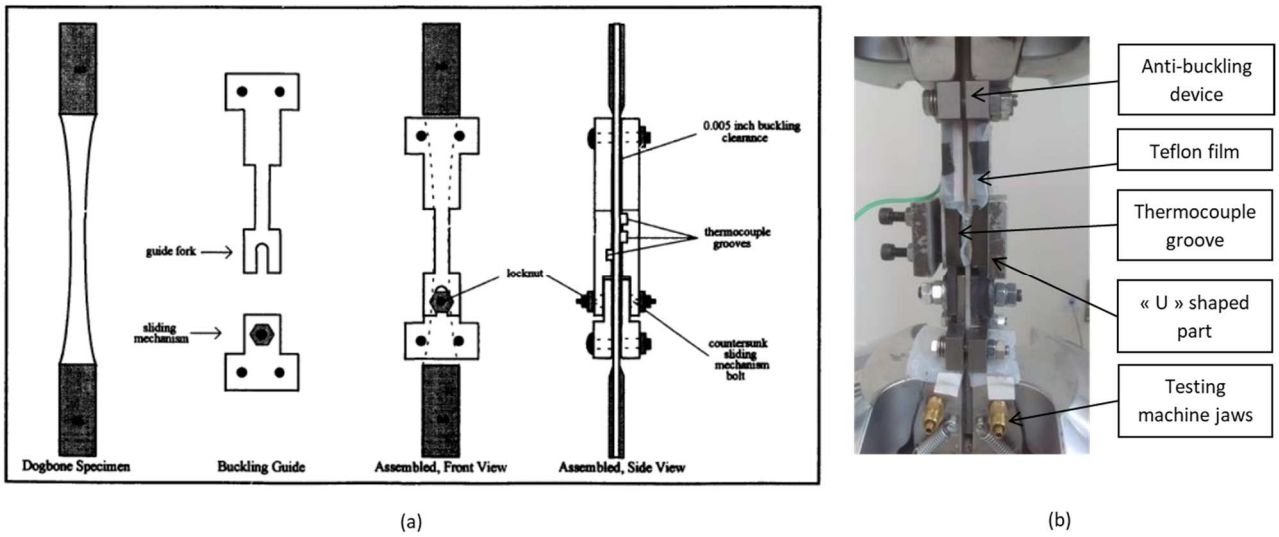

Figure 10: (a) Previous design of the anti-buckling device [56] and (b) its new design used for fatigue tests at R=-1 (tensile-compressive loading) on UD $[0]_4$ and BXS $[(\pm 45)_2]_s$ specimens

As shown in Figure 11, a set of parameters was found to satisfactorily predict both fatigue strength and damage evolution in the fibre direction. It is also true under a fatigue loading causing mainly shear stresses at the ply scale, as shown in Figure 12. The identified parameter values are given in Table 4. On the grounds of these results, the authors are confident that a suitable set of parameters can be found to predict satisfactorily both

fatigue strength and matrix damage evolution under a fatigue loading causing both shear and transverse stresses at the ply scale (i.e. all the parameters of Equation (17) are identified).

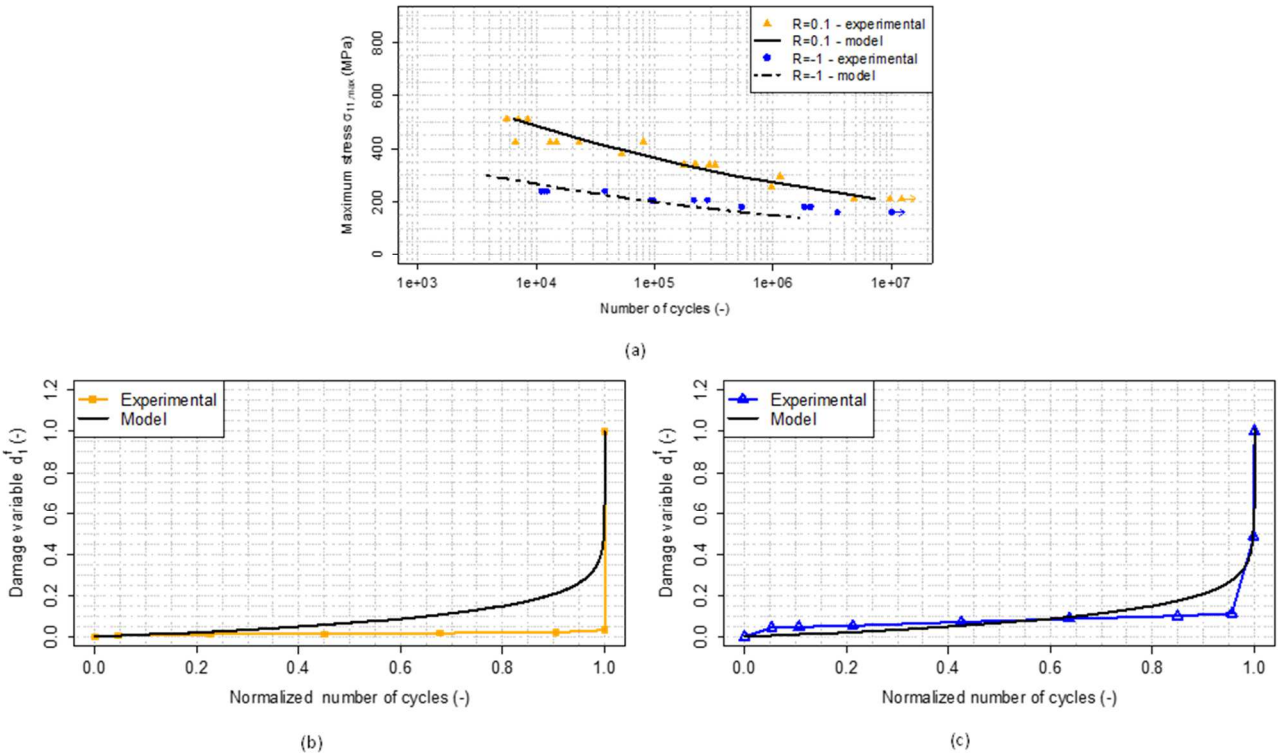

Figure 11: Comparison between experimental data at $R = 0.1$ *and* $R = -1$ *obtained from UD* $[0]_4$ *specimens and the model prediction of (a) ply fatigue strength in the fibre direction, (b) cumulative damage evolution at a maximum stress of 340MPa at* $R = 0.1$, $f = 5Hz$ *and* $V_f = 58\%$ *and (c) cumulative damage evolution at a maximum stress of 240MPa at* $R = -1$, $f = 3Hz$ *and* $V_f = 55\%$

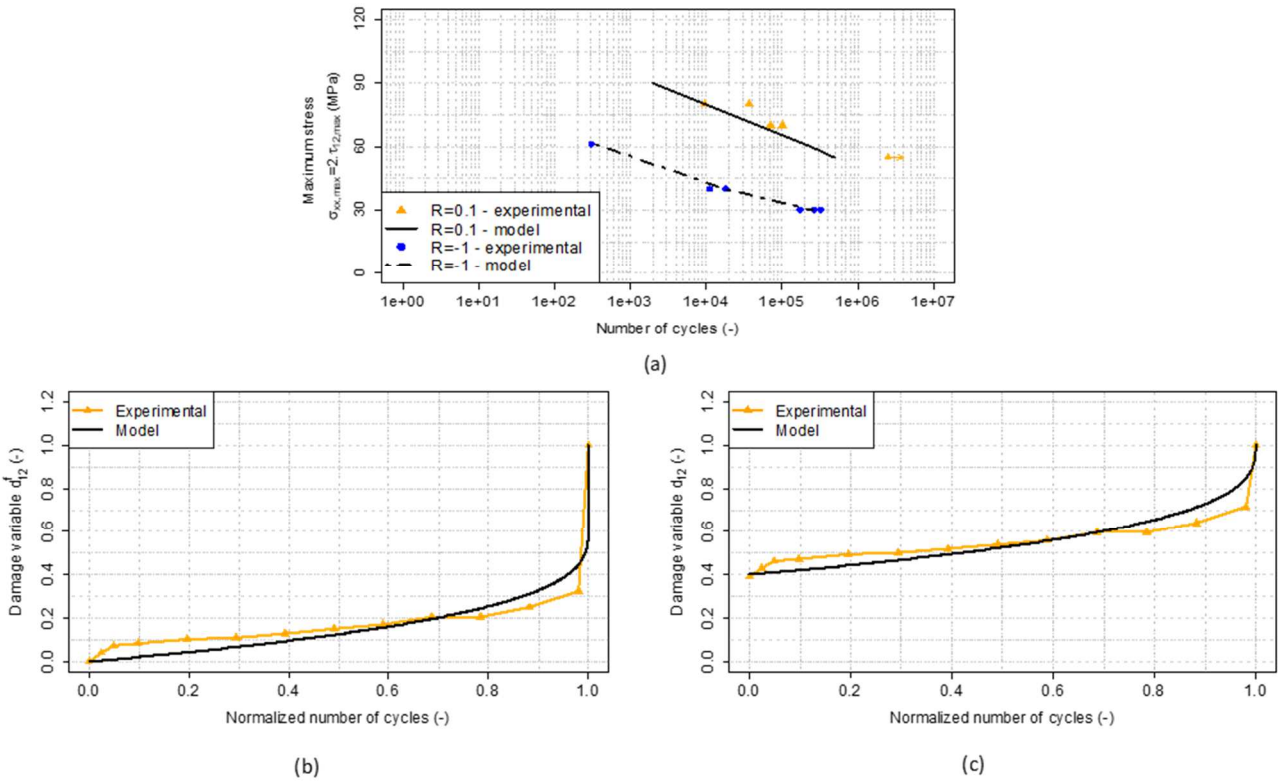

Figure 12: Comparison between experimental data at $R = 0.1$ and $R = -1$ obtained from BXS $[(\pm45)_2]_s$ specimen and the model prediction of (a) ply fatigue strength in the matrix-dominated behaviour under a fatigue loading causing mainly shear stresses at the ply scale, (b) fatigue damage evolution and (c) cumulative damage evolution at a maximum stress of 70MPa, at $R = 0.1$, $f = 5Hz$ and $V_f = 52\%$

Parameters	Test specimens	Identified values
$a_1\ (MPa^{-l_1-l_2})$		3.10^{-7}
$\gamma_1\ (-)$	UD $[0]_4$	-1
$l_1\ (-)$	($V_f = 55.6 \pm 2.0\%$)	1
$l_2\ (-)$		3
$b_2\ (MPa^{-n_1-n_2})$		2.10^{-2}
$\gamma_2\ (-)$	BXS $[(\pm45)_2]_s$	6
$n_1\ (-)$	($V_f = 52.8 \pm 1.6\%$)	0
$n_2\ (-)$		4

Table 4: Identified values for parameters of the damage evolution laws under a fatigue loading (cf. Equation (17))

4.4 Conclusion on the model identification

As mentioned before, the damage and plastic strain evolution laws used in this paper were initially proposed for thermoset-matrix laminates reinforced with glass fibres [32,52]. The study conducted here revealed that these evolution laws are suitable for acrylic-thermoplastic-matrix and glass-fibre-reinforced laminates used in

wind turbine blades with parameters identified at a given testing temperature. This result is of interest since previous studies showed that damage evolution laws used for thermoset-matrix laminates reinforced with carbon fibres were not suitable for those reinforced with glass fibres [36,38,49,52]. However, as mentioned in section 2 of this paper, the off-axis mechanical behaviour of this thermoplastic-matrix laminate depends significantly on the temperature in the service range of wind turbine blades. This is a real issue to ensure the accurate design of wind turbine blades made with such a material. Thus, the next part of this study focuses on proposing a simple way to model the temperature effect on the composite transverse and off-axis mechanical behaviour.

5 Taking into account the temperature effect on composite mechanical behaviour

First, the matrix initial elastic properties, E_m^0 and G_m^0, were identified at several testing temperatures from quasi-static tensile tests performed on UD $[90]_4$ specimens via the mixture laws for composites (Equations (20)). Results presented in Figure 13 show, as expected, that these two properties are temperature-dependent as they decrease with the increase in temperature. Even if the values of G_m^0 and E_m^0 obtained at 40°C with a single test do not give the same value for the Poisson's ratio ν_m^0 as those obtained at 15 and 20°C using Equation (21), we assume that Poisson's ratio is temperature-independent. In fact, the value of E_m^0 obtained at 40°C seems to be overestimated. It was therefore reassessed using Equation (21) and the value of ν_m^0 identified at 20°C (cf. Table 2). Following the same reasoning process, values of E_m^0 at 48°C and G_m^0 at 1°C were calculated.

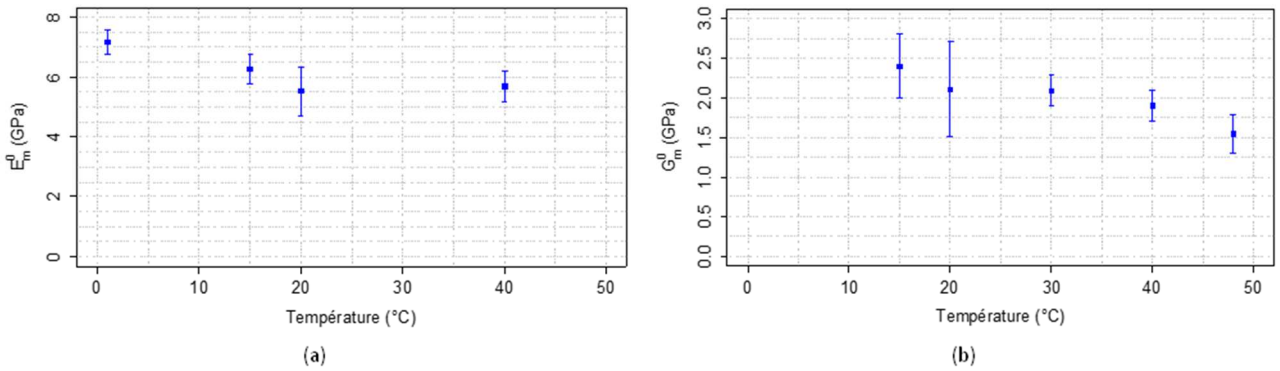

Figure 13: Temperature effect on matrix initial elastic properties (a) E_m^0 and (b) G_m^0, identified from quasi-static tensile tests on UD $[90]_4$ and $[(\pm 45)_2]_s$ specimens with $V_f = 58.5 \pm 0.7\%$ and $V_f = 51.3 \pm 0.7\%$ respectively

Parameters of the matrix damage and effective stress evolution laws (Equations (9) and (15)) for quasi-static loadings were identified at each testing temperature (cf. Table 5 for UD reinforcement and Table 6 for BXS reinforcement). Results show that these parameters seem poorly temperature-dependent. Moreover, as shown

in Figure 14 (a) [16,45], damage evolution against elastic strain under quasi-static tensile loading highlights no significant temperature effect. Thus, we choose to use an average value for each parameter for all testing temperatures. Regarding the matrix damage evolution law for fatigue loadings, which causes mainly shear stresses at the ply scale, Figure 14(b) shows that damage evolution against the number of cycles under fatigue loadings is also poorly temperature-dependent. Consequently, parameters b_2, γ_2, n_1 and n_2 (cf. Equation (26)) identified at 20°C were kept constant at the other two testing temperatures, 15 and 40°C. Hence, only the initial elastic modulus E_m^0 and the initial shear elastic modulus G_m^0 of the matrix were considered temperature-dependent for both types of loading. The model predictions were obtained using the discrete experimental values of E_m^0 and G_m^0.

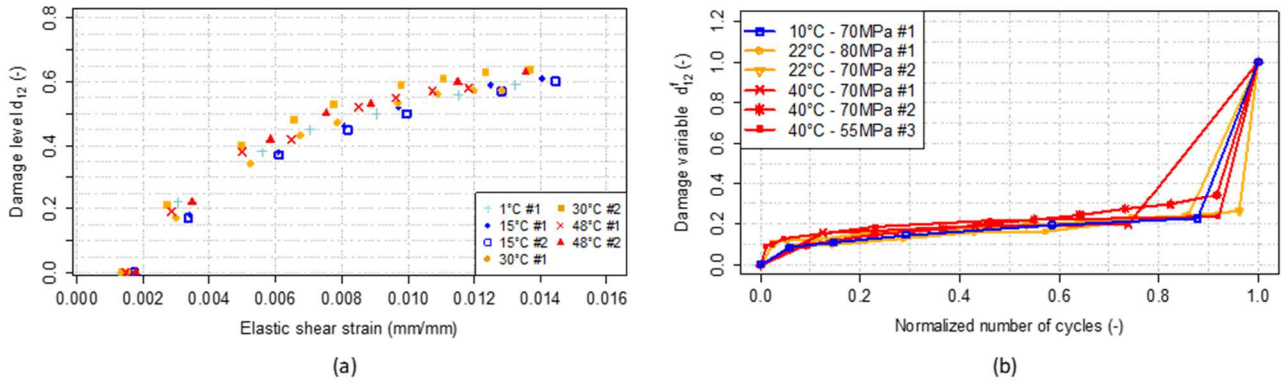

Figure 14: Damage evolution at different testing temperatures (a) against elastic strain under quasi-static tensile loadings for BXS $[(\pm45)_2]_s$ specimens with $V_f = 51.3 \pm 0.7\%$ [16,45] and (b) against the number of cycles under fatigue loadings at $R = 0.1$ at different maximum stress for UD $[(+45/-45)_2]_s$ specimens with $V_f = 52.9 \pm 1.3\%$

Parameters	1°C	15°C	20°C	40°C	Mean values
$b\ (MPa^{-m})$	/	1.45 ± 0.17	1.46 ± 0.04	1.87 ± 0.14	1.62 ± 0.24
$Y_0\ (-)$	/	0.20 ± 0.01	0.20 ± 0.01	0.21 ± 0.02	0.20 ± 0.01
$K(MPa)$	/	1063 ± 102	1015 ± 389	1024 ± 103	1029 ± 26
$\gamma\ (-)$	/	0.44 ± 0.04	0.46 ± 0.03	0.50 ± 0.01	0.47 ± 0.03
$R_0(MPa)$	/	0.00 ± 0.00	0.00 ± 0.00	0.00 ± 0.00	0.00 ± 0.00
$a\ (MPa^{-m})$	0.97 ± 0.30	1.40 ± 0.20	2.47 ± 1.62	2.11 ± 0.20	1.97 ± 0.68
$m\ (-)$	0.37 ± 0.09	0.39 ± 0.10	0.81 ± 0.26	0.53± 0.10	0.64 ± 0.52
$\alpha\ (-)$	0.43 ± 0.10	0.42 ± 0.10	0.86 ± 0.13	0.49 ± 0.10	0.74 ± 0.55

Table 5: Mean values identified for the parameters of the matrix damage and effective stress evolution laws for quasi-static loadings at 15, 20 and 40°C on UD reinforcement and mean values for each parameter over all the testing temperatures

Parameters	1°C	15°C	20°C	30°C	48°C	Mean values
$b\ (MPa^{-m})$	0.78 ± 0.30	1.45 ± 0.15	0.88 ± 0.20	0.95 ± 0.30	2.39 ± 0.24$^{(*)}$	1.29 ± 0.30
$Y_0\ (-)$	0.30 ± 0.02	0.22 ± 0.02	0.10 ± 0.00	0.08 ± 0.02	0.30 ± 0.03	0.15 ± 0.11
$K(MPa)$	1411 ± 200	2221 ± 350	542 ± 300	1206 ± 550	1326 ± 850	1341 ± 599
$\gamma\ (-)$	0.48 ± 0.10	0.58 ± 0.10	0.40 ± 0.10	0.50 ± 0.07	0.58 ± 0.11	0.51 ± 0.07
$R_0(MPa)$	0.00 ± 0.00	0.00 ± 0.00	0.00 ± 0.00	0.00 ± 0.00	0.00 ± 0.00	0.00 ± 0.00

Table 6: Mean values identified for the parameters of the matrix damage and effective stress evolution laws for quasi-static loadings at 1, 15, 20, 30 and 48°C on BXS reinforcement and mean values for each parameter over all the testing temperatures – (*) value not considered in the calculation of the mean value because too far from the values at the other testing temperatures

As shown in Figure 15 for quasi-static loadings, under this assumption, the model gives a good prediction of the mechanical behaviour of UD $[90]_4$ lamination, regardless of the testing temperature, up to a strain of about 0.4%. Thus, assuming that only the matrix elastic properties are temperature-dependent works for this lamination, between 1 and 40°C. For BXS $[(\pm45)_2]_s$, UD $[(+45/-45)_2]_s$ and UD $[(+60/-60)_2]_s$ lamination, the model overestimates the damage evolution, except at 30°C and 48°C for BXS $[(\pm45)_2]_s$ lamination (see Figure 16, Figure 17, and Figure 18 respectively). These results highlight that the damage model struggles to represent some phenomena involved in the damage process of the composite under investigation with UD reinforcement. The UD reinforcement is in fact a very unbalanced reinforcement (see Table 1). Glass fibres in the weft direction allow for gradual damage growth in the transverse direction, while the first transverse crack classically leads to ply failure for purely UD ply. Consequently, the variant of the damage model developed by Hochard et al. [37] for woven unbalanced reinforcement might be more appropriate for this type of reinforcement. However, that would involve using two different models and sets of parameters for the two types of reinforcement. For BXS reinforcement, results show that the values of parameters a, m, and α identified on UD reinforcement for the evolution of damage in the transverse direction may not be adequate. These observations are consistent with the fact that decreasing the values of parameters b and a to 1.00 and 1.20, respectively, significantly improved the model prediction for these laminations, regardless of the testing temperature (dotted lines in Figure 16, Figure 17 and Figure 18). The sole exception is at 48°C for BXS $[(\pm45)_2]_s$ lamination, which is directly linked to the fact that the value identified for the b parameter is 1.9 times

higher than the mean value at all the other testing temperatures (Table 6). This implies that taking one set of parameters for all testing temperatures and considering only the initial elastic modulus E_m^0 and the initial shear elastic modulus G_m^0 of the matrix as temperature-dependent also works satisfactorily for BXS $[(\pm45)_2]_s$, UD $[(+45/-45)_2]_s$ and UD $[(+60/-60)_2]_s$ laminations. The issue remains concerning the identification of b and a parameters. Since decreasing them to 1.00 and 1.20, respectively, worsens the model prediction for UD $[90]_4$ lamination (Figure 15), a compromise has to be found for the b and a values so that the chosen damage model gives satisfactory predictions simultaneously for UD $[90]_4$ lamination and BXS $[(\pm45)_2]_s$, UD $[(+45/-45)_2]_s$ and UD $[(+60/-60)_2]_s$ laminations. Concerning fatigue loadings, the values of parameters b and a have little influence on model predictions since the stress and damage level due to the monotonic loading are quite low. Figure 19 shows the model predictions of the shear fatigue strength at 15°C and 40°C. Keeping in mind that fatigue tests generally exhibit scattered results, the prediction seems to agree with the experimental results and to succeeds in representing the effect of temperature. However, supplementary fatigue tests at both 15 and 40°C, and above all at 15°C, reaching between 10^5 and 10^6 cycles, will be useful to confirm this capability. Thus, considering only the initial elastic properties of the matrix as temperature-dependent seems sufficient to be able to simulate the composite service life across the entire temperature service range of wind turbine blades, but this needs to be corroborated.

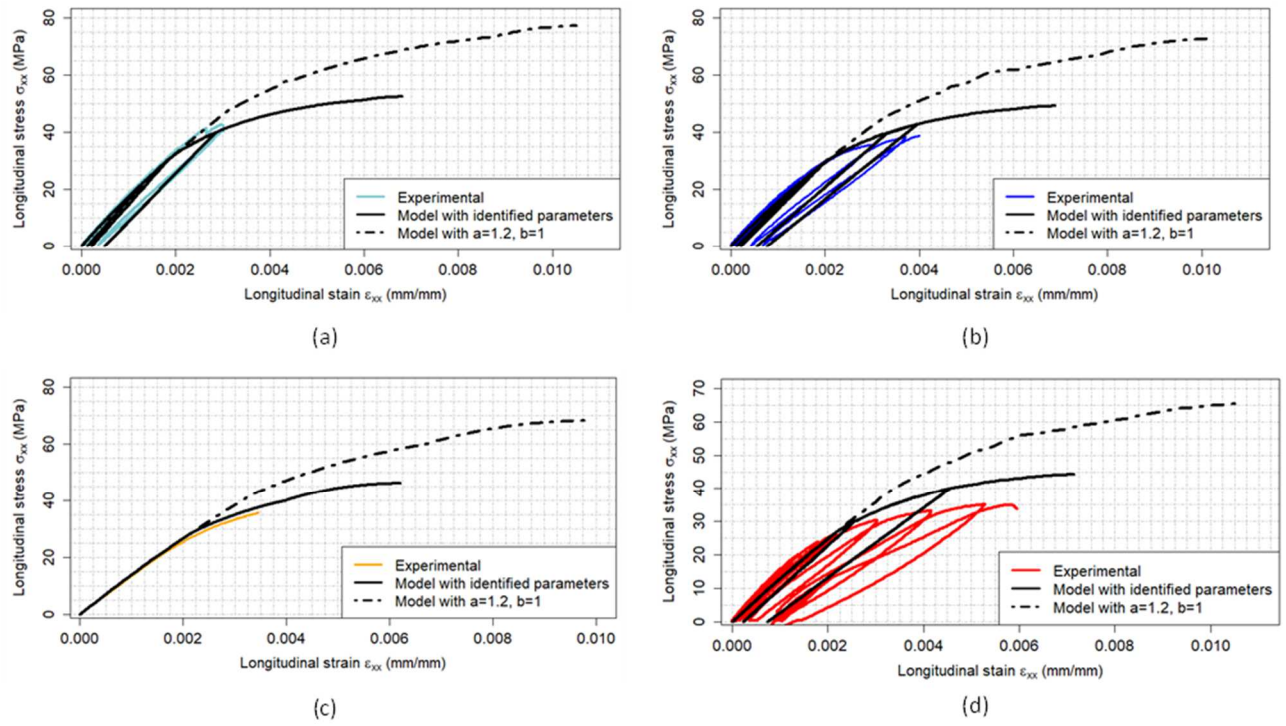

Figure 15: Comparison between experiments and model predictions of the mechanical behaviour of UD $[90]_4$ lamination under a tensile loading with only E_m^0 and G_m^0 considered as temperature-dependent parameters at (a) 1°C - $V_f = 58.7\%$, (b) 15°C - $V_f = 58.2\%$, (c) 20°C - $V_f = 57.8\%$ and (d) 40°C - $V_f = 57.6\%$

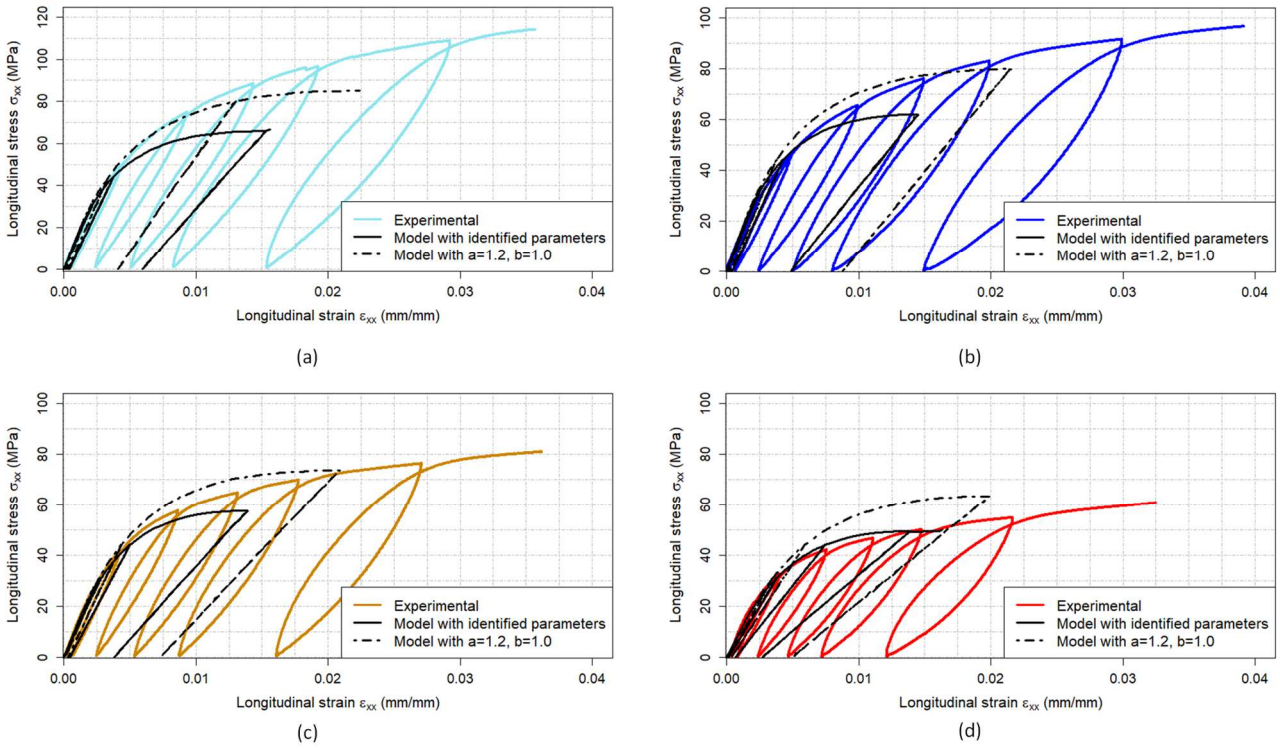

Figure 16: Comparison between experiments and model predictions of the mechanical behaviour of BXS $[(\pm 45)_2]_s$ lamination under a quasi-static tensile loading with only E_m^0 and G_m^0 considered as temperature-dependent parameters at (a) 1°C - $V_f = 51.8\%$, (b) 15°C - $V_f = 51.5\%$, (c) 30°C - $V_f = 51.1\%$ and (d) 48°C - $V_f = 50.7\%$

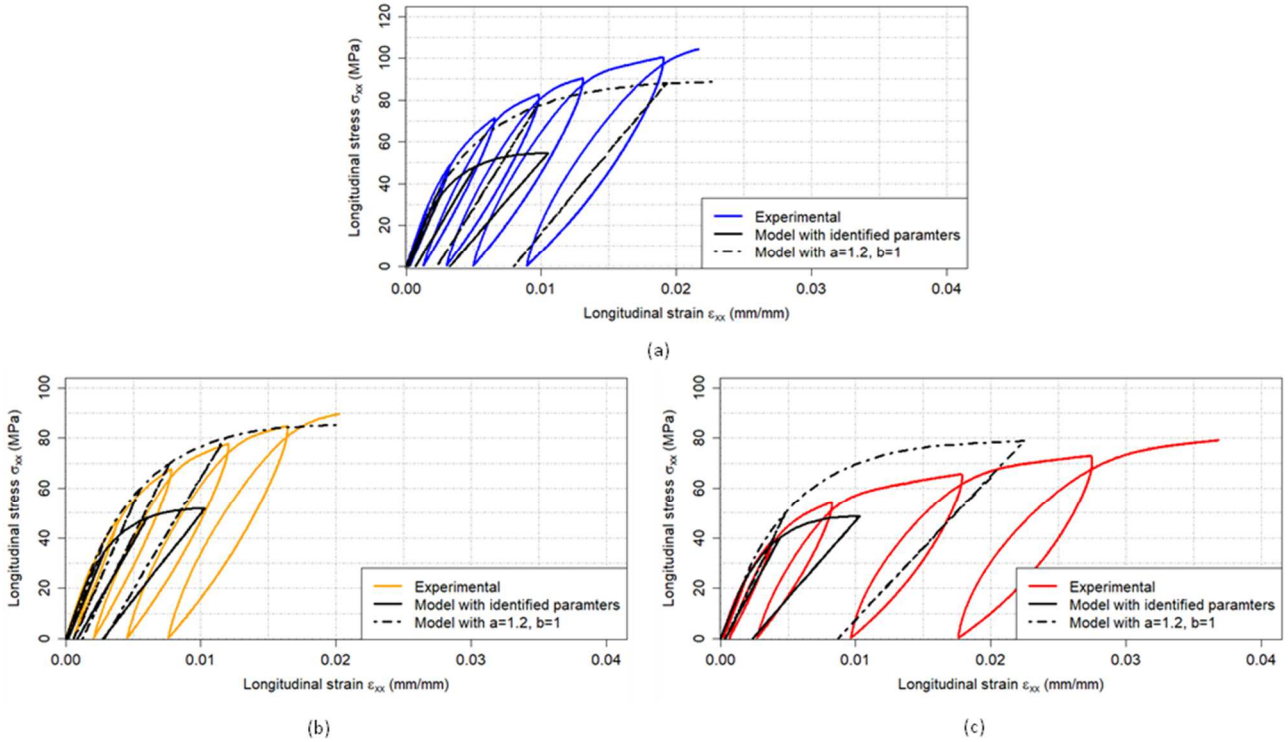

Figure 17: Comparison between experiments and model predictions of the mechanical behaviour of UD $[(+45/-45)_2]_s$ lamination under a quasi-static tensile loading with only E_m^0 and G_m^0 considered as temperature-dependent parameters at (a) 15°C - $V_f = 55.7\%$, (b) 20°C - $V_f = 56.2\%$ and (c) 40°C - $V_f = 55.8\%$

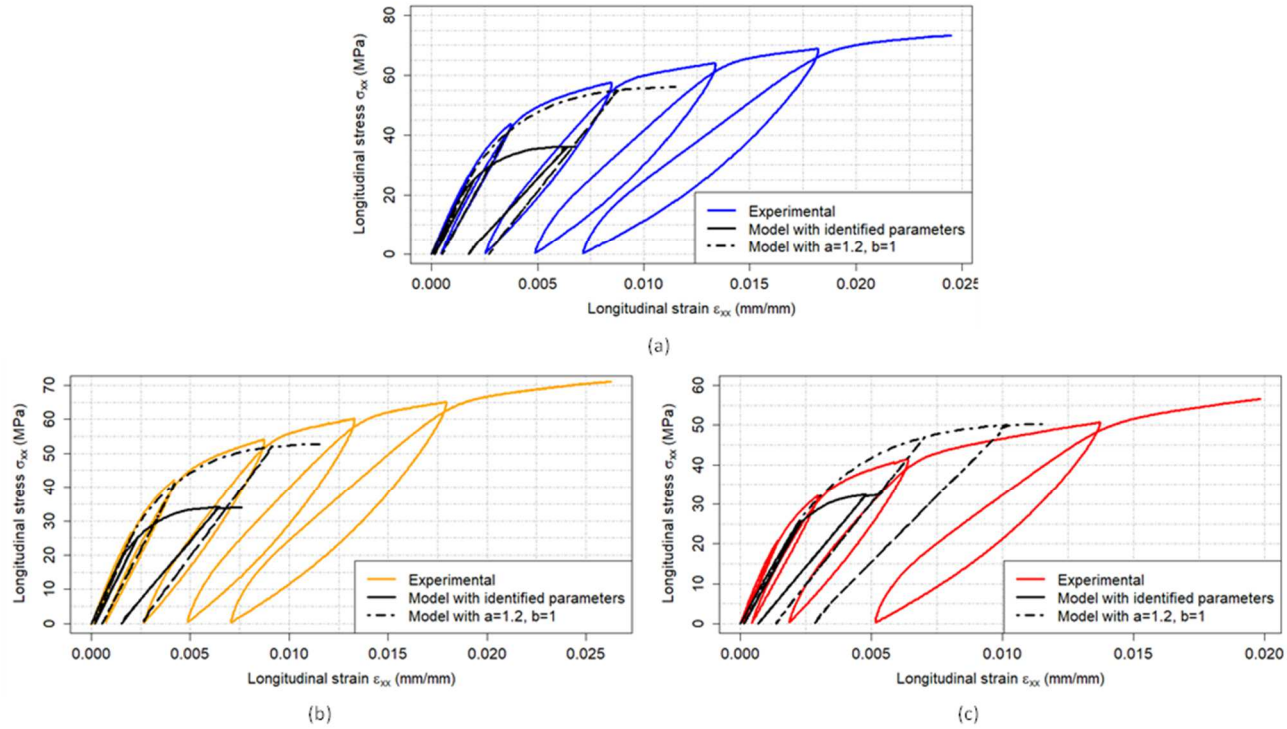

Figure 18: Comparison between experiments and model predictions of the mechanical behaviour of UD $[(+60/-60)_2]_s$ lamination under a tensile loading with only E_m^0 and G_m^0 considered as temperature-dependent parameters at (a) 15°C - $V_f = 58.1\%$, (b) 20°C - $V_f = 58.1\%$ and (c) 40°C - $V_f = 58.0\%$

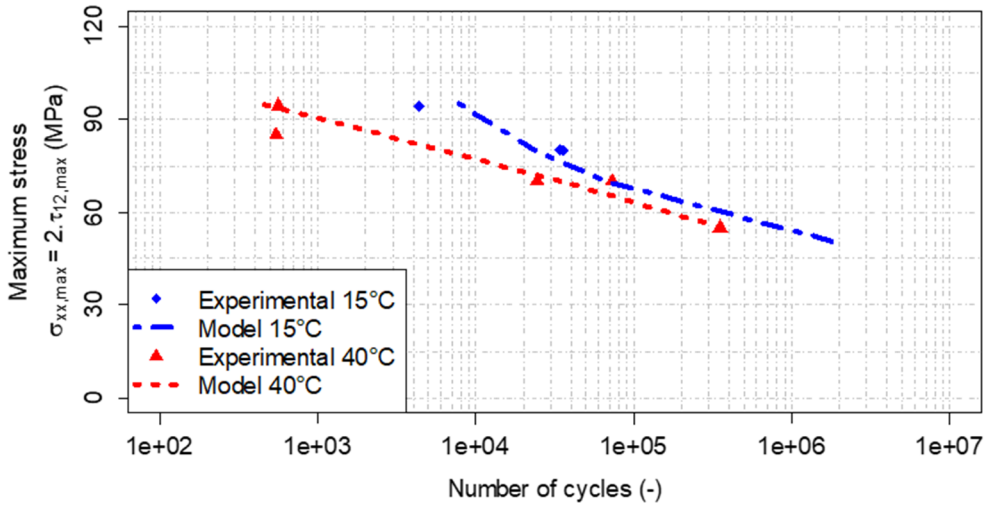

Figure 19: Comparison between experiments and model predictions of the composite fatigue strength of BXS $[(\pm 45)_2]_s$ specimens at 15 and 36°C with only E_m^0 and G_m^0 considered as temperature-dependent parameters

6 Conclusion and prospects for future studies

In this paper, a model formulated at the ply scale was considered to describe the mechanical behaviour of an acrylic-thermoplastic-matrix and glass-fibre-reinforced laminated composite under quasi-static tensile and fatigue loadings. This model had been successfully used in previous studies to predict satisfactorily the mechanical behaviour of laminated composites with a thermoset-matrix and either glass or carbon fibres [32,36,38,52]. First, the study at room temperature revealed that this model is suitable for the laminate under investigation without any change in the evolution laws (as it was done between carbon-fibre-reinforced and glass-fibre-reinforced composites with thermoset matrix) even if the variant of the model purposed by Hochard et al. [37] is used for the UD reinforcement as it is in fact a very unbalanced fabric. Despite this, this study showed that the temperature dependency of the composite transverse and off-axis mechanical behaviour could be achieved more simply, by considering only the temperature dependency of the initial elastic properties of the matrix (i.e. fibre initial elastic properties and damage evolution law parameters are kept constant). This is a relevant result for the industrial field for a better design of wind turbine blades using such an innovative composite material. However, it has to be noted that it is achievable because damage and plastic strain evolution against strain level under a tensile loading and damage evolution against the normalized cycle number under a fatigue loading are poorly temperature-dependent in the temperature range under consideration [15], i.e. from -20°C to 60°C.

As mentioned in the introduction, wind turbine blades undergo 10^8-10^9 fatigue cycles during their 20-year lifetime. However, fatigue tests performed in this study were conducted up to 10^7 fatigue cycles at most, due to the significant self-heating capacity of the composite under investigation. It must remain at a maximum frequency of 10Hz to maintain a maximum specimen self-heating of 5°C. This criterion was chosen because the temperature effect is studied here in a narrow range. Thus, a study of fatigue strength and damage evolution over a very long lifetime is needed, which will be more representative of the loading undergone by wind turbine blades. It would also be interesting to extend the model validity domain to marine renewable energies, especially to marine turbines, by studying the ageing impact - and more specifically the water-ageing impact - on the mechanical behaviour of polymer composites under tensile and fatigue loadings.

Finally, by developing a micromechanical approach introducing active phenomena at the material scale it would be possible to study matrix behaviour more closely, looking at composite microstructure interaction for a better understanding of the phenomenology. As a second step, this kind of approach may make it possible to

push forward and identify the meso-scale damage model. Such studies can already be found in the literature, but they are facing two major issues related to identifying a mechanical behaviour that is representative of that of the matrix once in the composite, and to building microstructures representative of composite behaviour regarding spatial variability.

7 Acknowledgments

The authors thank the Nouvelle Aquitaine region, ADEME and all the partners in the EFFIWIND project for their support. The EFFIWIND project has been chosen by the regional council of Nouvelle Aquitaine and ADEME for funding as part of the French Investissements d'Avenir program.

8 References

[1] C. Bathias, Matériaux Composites, Dunod, France, 2005.
[2] M.N. Bureau, J. Denault, Fatigue resistance of continuous glass fiber/polypropylene composites: consolidation dependence, Composites Science and Technology. 64 (2004) 1785–1794.
[3] J.F. Mandell, R.M. Reed, D.D. Samborsky, Fatigue of fiberglass wind turbine blade materials, Sandia National Laboratories, USA, 1992.
[4] R.P.L. Nijssen, Fatigue Life Prediction and Strength Degradation of Wind Turbine Rotor Blade Composites, PhD Thesis, Delft University of Technology, 2007.
[5] J.R. Calcaterra, S. Mall, Strength degradation during fatigue of unidirectional and cross-ply SCS-6/Ti-15-3 composites, International Journal of Fatigue. 21 (1999) 215–223. https://doi.org/10.1016/S0142-1123(98)00068-1.
[6] G.N. Praveen, J.N. Reddy, Transverse matrix cracks in cross-ply laminates: Stress transfer, stiffness reduction and crack opening profiles, Acta Mechanica. 130 (1998) 227–248. https://doi.org/10.1007/BF01184313.
[7] N. Revest, Comportement en fatigue de pièces épaisses en matériaux composites, PhD Thesis, Ecole nationale supérieure des Mines de Paris, 2011.
[8] K.I. Tserpes, P. Papanikos, G. Labeas, S. Pantelakis, Fatigue damage accumulation and residual strength assessment of CFRP laminates, Composite Structures. 63 (2004) 219–230. https://doi.org/10.1016/S0263-8223(03)00169-7.
[9] G. Eyer, O. Montagnier, C. Hochard, J.-P. Charles, Effect of matrix damage on compressive strength in the fiber direction for laminated composites, Composites Part A: Applied Science and Manufacturing. 94 (2017) 86–92. https://doi.org/10.1016/j.compositesa.2016.12.012.
[10] D. Caous, C. Bois, J.-C. Wahl, T. Palin-Luc, J. Valette, A method to determine composite material residual tensile strength in the fibre direction as a function of the matrix damage state after fatigue loadings, Composite Part B: Engineering. 127 (2017) 15–25.
[11] E. Riande, R. Diaz-Calleja, M. Prolongo, R. Masegosa, C. Salom, Polymer Viscoelasticity: Stress and Strain in Practice, CRC Press, 1999.
[12] J. Montesano, M. Selezneva, Z. Fawaz, C. Poon, K. Behdinan, Elevated temperature off-axis fatigue behavior of an eight-harness satin woven carbon-fiber/bismaleimide laminate, Composites Part A: Applied Science and Manufacturing. 43 (2012) 1454–1466. https://doi.org/10.1016/j.compositesa.2012.04.016.
[13] L. Sorrentino, D.S. de Vasconcellos, M. D'Auria, F. Sarasini, J. Tirillò, Effect of temperature on static and low velocity impact properties of thermoplastic composites, Composites Part B: Engineering. 113 (2017) 100–110. https://doi.org/10.1016/j.compositesb.2017.01.010.
[14] H. Mivehchi, A. Varvani-Farahani, The effect of temperature on fatigue strength and cumulative fatigue damage of FRP composites, Procedia Engineering. 2 (2010) 2011–2020. https://doi.org/10.1016/j.proeng.2010.03.216.

[15] E. Boissin, Etude de l'endommagement et de la tenue en fatigue d'un composite à matrice acrylique et fibres de verre, PhD Thesis, Université de Bordeaux, 2019.
[16] E. Boissin, C. Bois, J.-C. Wahl, T. Palin-Luc, Effect of temperature on damage mechanisms and mechanical behaviour of an acrylic-thermoplastic-matrix and glass-fibre-reinforced composite, Journal of Composite Materials. Accepted Manuscript (2020).
[17] L. Cadieu, J.B. Kopp, J. Jumel, J. Bega, C. Froustey, Temperature effect on the mechanical properties and damage mechanisms of a glass/thermoplastic laminate, Journal of Composite Materials. 54 (2020) 2271–2282. https://doi.org/10.1177/0021998319894383.
[18] L. Cadieu, J.B. Kopp, J. Jumel, J. Bega, C. Froustey, A fracture behaviour evaluation of Glass/Elium150 thermoplastic laminate with the DCB test: Influence of loading rate and temperature, Composite Structures. 255 (2021) 112907. https://doi.org/10.1016/j.compstruct.2020.112907.
[19] EFFIWIND project: First 25m long wind blade manufactured using ELIUM resin, Plateforme Canoe EN. (2018). http://www.plateforme-canoe.com/en/effiwind-project-first-25m-long-wind-blade-manufactured-using-elium-resin/ (accessed April 15, 2020).
[20] C.P. Debel, Identification of damage types in wind turbine blades tested to failure, in: Materialeopførsel Og Skadesanalyse, Dansk Metallurgisk Selskab, 2004: pp. 123–127. https://orbit.dtu.dk/en/publications/identification-of-damage-types-in-wind-turbine-blades-tested-to-f (accessed June 2, 2021).
[21] E.R. Jørgensen, K.K. Borum, M. McGugan, C.L. Thomsen, F.M. Jensen, C.P. Debel, B.F. Sørensen, Full scale testing of wind turbine blade to failure - flapwise loading, Risø National Laboratory, Denmark, 2004. https://orbit.dtu.dk/en/publications/full-scale-testing-of-wind-turbine-blade-to-failure-flapwise-load (accessed June 2, 2021).
[22] B.F. Sørensen, E.R. Jørgensen, C.P. Debel, F.M. Jensen, H.M. Jensen, T.K. Jacobsen, K.M. Halling, Improved design of large wind turbine blade of fibre composites based on studies of scale effects (Phase 1) - Summary Report, Risø National Laboratory, Denmark, 2004.
[23] J. Epaarachchi, P. Clausen, Accelerated Full Scale Fatigue Testing Of A Small Composite Wind Turbine Blade Using A Mechanically Operated Test Rig, in: Tructural Integrity and Fracture International Conference (SIF2004), Australia, 2004.
[24] M.A. Rumsey, J.A. Paquette, Structural health monitoring of wind turbine blades, in: Smart Sensor Phenomena, Technology, Networks, and Systems 2008, International Society for Optics and Photonics, 2008: p. 69330E. https://doi.org/10.1117/12.778324.
[25] F.-M. Lai, S.-H. Yang, J.-H. Wu, C.-T. Hsueh, C.-C. Yang, B.-H. Wang, C.-H. Lan, Development of Fatigue Test System for Small Composite Wind Turbine Blades, Procedia Engineering. 14 (2011) 2003–2013. https://doi.org/10.1016/j.proeng.2011.07.252.
[26] S.G. Taylor, K.M. Farinholt, H. Jeong, J.-K. Jang, G. Park, M.D. Todd, C.R. Farrar, C.M. Ammerman, Wind Turbine Blade Fatigue Tests: Lessons Learned and Application to SHM System Development, in: 6th European Workshop on Structural Health Monitoring, Dresden, Germany, 2012: p. 8.
[27] CENER, International statistical analysis on wind turbine failures, in: 67th IEA Topical Expert Meeting, Kassel, Germany, 2011.
[28] J.-S. Chou, C.-K. Chiu, I.-K. Huang, K.-N. Chi, Failure analysis of wind turbine blade under critical wind loads, Engineering Failure Analysis. 27 (2013) 99–118. https://doi.org/10.1016/j.engfailanal.2012.08.002.
[29] Caithness Windfarm Information Forum 2021, Summary of Wind Turbine Accident, (n.d.). http://www.caithnesswindfarms.co.uk/AccidentStatistics.htm (accessed June 2, 2021).
[30] IEC 61400-1 Wind turbines Part 1: Design requirements, (2005).
[31] Germanischer Lloyd, Guideline for the Certification of Wind Turbines, Germanischer Lloyd, 2010.
[32] D. Caous, Role of damage on the fatigue life of laminated composite materials: application to the wind industry, PhD Thesis, Université Bordeaux, 2017.
[33] D.T. Griffith, T.D. Ashwill, The Sandia 100-meter All-glass Baseline Wind Turbine Blade: SNL100-00, (n.d.) 67.
[34] S.N. Laboratories, Sandia National Laboratories: News Releases: Enormous Blades Could Lead to More Offshore Energy in U.S., Power Electronics. (2016). https://www.powerelectronics.com/technologies/alternative-energy/article/21863279/enormous-blades-could-lead-to-more-offshore-energy-in-us (accessed June 2, 2021).
[35] The Maritime Executive, World's Longest Wind Turbine Blade Revealed, The Maritime Executive. (n.d.). https://www.maritime-executive.com/article/world-s-longest-wind-turbine-blade-revealed (accessed June 2, 2021).

[36] J. Payan, C. Hochard, Damage modelling of laminated carbon/epoxy composites under static and fatigue loadings, International Journal of Fatigue. 24 (2002) 299–306.
[37] Ch. Hochard, Y. Thollon, A generalized damage model for woven ply laminates under static and fatigue loading conditions, International Journal of Fatigue. 32 (2010) 158–165. https://doi.org/10.1016/j.ijfatigue.2009.02.016.
[38] P. Ladeveze, E. LeDantec, Damage modelling of the elementary ply for laminated composites, Composites Science and Technology. 43 (1992) 257–267.
[39] C. Rakotoarisoa, F. Laurin, M. Hirsekorn, J.-F. Maire, L. Olivier, Development of a fatigue model for 3D woven polymer matrix composites based on a damage model, in: 2012. https://www.scopus.com/inward/record.uri?eid=2-s2.0-84903954367&partnerID=40&md5=5ea652ae784b7cfe2a11e1c746b074ed.
[40] F. Laurin, N. Carrere, C. Huchette, J.-F. Maire, A multiscale hybrid approach for damage and final failure predictions of composite structures, Journal of Composite Materials. 47 (2013) 2713–2747. https://doi.org/10.1177/0021998312470151.
[41] F. Praud, G. Chatzigeorgiou, Y. Chemisky, F. Meraghni, Hybrid micromechanical-phenomenological modelling of anisotropic damage and anelasticity induced by micro-cracks in unidirectional composites, Composite Structures. 182 (2017) 223–236. https://doi.org/10.1016/j.compstruct.2017.09.013.
[42] F. Naya, C. González, C.S. Lopes, S. Van der Veen, F. Pons, Computational micromechanics of the transverse and shear behavior of unidirectional fiber reinforced polymers including environmental effects, Composites Part A: Applied Science and Manufacturing. 92 (2017) 146–157. https://doi.org/10.1016/j.compositesa.2016.06.018.
[43] H. Wang, B. Sun, B. Gu, Numerical modeling on compressive behaviors of 3-D braided composites under high temperatures at microstructure level, Composite Structures. 160 (2017) 925–938. https://doi.org/10.1016/j.compstruct.2016.10.130.
[44] A.P. Vassilopoulos, 1 - Introduction to the fatigue life prediction of composite materials and structures: past, present and future prospects, in: A.P. Vassilopoulos (Ed.), Fatigue Life Prediction of Composites and Composite Structures, Woodhead Publishing, 2010: pp. 1–44. https://doi.org/10.1533/9781845699796.1.
[45] E. Boissin, C. Bois, J.-C. Wahl, T. Palin-Luc, Effect of temperature on damage mechanisms in an acrylic-matrix and glass-fibre-reinforced composite under monotonic tensile and fatigue loadings, in: 18th European Conference on Composite Materials (ECCM18), Athens, Greece, 2018.
[46] I. De Baere, W. Van Paepegem, C. Hochard, J. Degrieck, On the tension–tension fatigue behaviour of a carbon reinforced thermoplastic part II: Evaluation of a dumbbell-shaped specimen, Polymer Testing. 30 (2011) 663–672. https://doi.org/10.1016/j.polymertesting.2011.05.005.
[47] J. Montesano, Z. Fawaz, C. Poon, K. Behdinan, A microscopic investigation of failure mechanisms in a triaxially braided polyimide composite at room and elevated temperatures, Materials & Design. 53 (2014) 1026–1036. https://doi.org/10.1016/j.matdes.2013.08.003.
[48] W. Tsai, Introduction to Composite Materials, Air Force Materials Laboratory, USA, 1979.
[49] J. Payan, Etude du comportement de composites stratifiés sous chargement statique et de fatigue, Aix-Marseille, 2004. \\Tsl-data\developpement\1-R&DInt\5-Endommagement\3-THESE\1c-Biblio\5-Theses\These_Payan_ComportementStratifiesStatiqueFatigue_2004.pdf.
[50] C. Hochard, J. Payan, C. Bordreuil, A progressive first ply failure model for woven ply CFRP laminates under static and fatigue loads, International Journal of Fatigue. 28 (2006) 1270–1276. https://doi.org/10.1016/j.ijfatigue.2006.04.002.
[51] S. Miot, Rupture de structures composites stratifiées sous chargement statique et de fatigue, PhD Thesis, Université Aix Marseille II, 2009.
[52] Ch. Hochard, St. Miot, Y. Thollon, Fatigue of laminated composite structures with stress concentrations, Composites Part B: Engineering. 65 (2014) 11–16. https://doi.org/10.1016/j.compositesb.2013.10.020.
[53] Ch. Hochard, P.-A. Aubourg, J.-P. Charles, Modelling of the mechanical behaviour of woven-fabric CFRP laminates up to failure, Composites Science and Technology. 61 (2001) 221–230. https://doi.org/10.1016/S0266-3538(00)00199-8.
[54] D. Gay, Composite Materials: Design and Applications, Third Edition, CRC Press, 2014.
[55] C.W. Kensche, Fatigue of composites for wind turbines, International Journal of Fatigue. 28 (2006) 1363–1374. https://doi.org/10.1016/j.ijfatigue.2006.02.040.
[56] E.A. Boyum, Investigation of Tension-Compression Fatigue Behavior of a Cross-Ply Metal Matrix Composite at Room and Elevated Temperatures, PhD Thesis, Faculty of the Graduate School of Engineering of the Air Force Institute of Technology, 1993.

[57] E.A. Boyum, S. Mall, Fatigue behavior of a cross-ply titanium matrix composite under tension-tension and tension-compression cycling, Materials Science and Engineering: A. 200 (1995) 1–11. https://doi.org/10.1016/0921-5093(95)07006-0.
[58] D.L. Kraabel, B.P. Sanders, S. Mall, Tension-compression fatigue behavior of a unidirectional titanium-matrix composite at elevated temperature, Composites Science and Technology. 57 (1997) 99–117. https://doi.org/10.1016/S0266-3538(96)00113-3.
[59] B.P. Sanders, S. Mall, S.C. Jackson, Load ratio effects on fatigue response of titanium matrix composite at elevated temperature, International Journal of Fatigue. 21 (1999) 121–134. https://doi.org/10.1016/S0142-1123(98)00059-0.